Joint Design of UAV Trajectory and Directional Antenna Orientation in UAV-Enabled Wireless Power Transfer Networks

Xiaopeng Yuan, Yulin Hu*, and Anke Schmeink

Abstract

In this work, we investigate an unmanned aerial vehicle (UAV)-enabled wireless power transfer (WPT) network with multiple ground sensor nodes (SNs). A UAV is operated at a fixed altitude with a directional antenna array and is designed to wirelessly transfer energy to the SNs. We consider a non-linear energy harvesting (EH) model and a directional antenna structure of uniform linear array (ULA) where we apply an analog directional beamforming scheme. Taking the fairness issue into account, we consider a problem aiming at maximizing the minimum harvested energy among all SNs during a fixed time period by jointly optimizing the UAV trajectory and the orientation of the directional antenna on the UAV. However, the complex antenna pattern expression of analog directional beamforming and the implicit non-linear function in the EH model introduce significant difficulties in handling the non-convex problem of the joint design. To tackle these difficulties, we propose and adopt a modified approximate antenna pattern model, i.e., a modified cosine antenna pattern, and reformulate the original problem via quantizing the UAV trajectory in the time domain. Later, by employing a convex property in the EH model and a proved lemma, we successfully construct a tight convex approximation for the reformulated problem, based on which the problem can be solved via a proposed iterative algorithm and the objective converges to an efficient suboptimal solution. Finally, we provide numerical results to confirm the convergence of the proposed algorithm, examine the approximation error and evaluate the system performance. The results show the performance advantage of the directional antenna in UAV-enabled WPT networks than the omni-directional antenna case, and illustrate how the directional antenna of the UAV overcomes its coverage limitation.

Part of this paper has been submitted to IEEE International Conference on Communications (ICC), June 2021, Montreal, Canada.

X. Yuan and Y. Hu are with School of Electronic Information, Wuhan University, 430072 Wuhan, China and ISEK Research Area, RWTH Aachen University, D-52074 Aachen, Germany. (Email:yuan@isek.rwth-aachen.de, yulin.hu@whu.edu.cn). *Y. Hu is the corresponding author.

A. Schmeink is with ISEK Research Area/Lab, RWTH Aachen University, D-52074 Aachen, Germany. (Email: schmeink@isek.rwth-aachen.de).

Index Terms

Unmanned aerial vehicle (UAV), nonlinear energy harvesting (EH), directional antenna, trajectory design, joint optimization.

I. Introduction

In recent years, the flexible deployment of unmanned aerial vehicles (UAVs) has enabled manifold applications in various scenarios, such as aerial monitoring, emergency assistance and cargo transportation [1], [2], and has consequently encouraged abundant related investigations. In UAV-aided wireless networks, due to the high probability of existence of line-of-sight(LoS) dominant air-ground channels, considerable benefits have been discovered in system evaluations, compared to the traditional terrestrial cellular networks [3]. In particular, the system performance can be enhanced via designing the deployment position of a UAV and the UAV trajectory [4]. While implementing the UAV as a mobile base station, researchers tried to improve the coverage [5]–[7], the channel capacity [8], [9] and the energy efficiency [10], [11]. Considering a UAV relay, the authors in [12] have studied the throughput maximization via optimizing the UAV trajectory. Furthermore, since the UAV is actually experiencing a changing communication environment when we deploy the mobility of a UAV, a joint optimization of the UAV trajectory and resource allocation regarding the variant channel states is generally recommended in UAV-assisted networks. For instance, a joint power control has been performed with a UAV trajectory design for secure communications in [13], [14] and for a higher reliability in relaying networks in [15]. In [16], the precoding process has been jointly optimized with a UAV trajectory by considering the maximization of the communication rate.

Besides, incorporating UAVs into wireless power transfer (WPT) networks has also attracted attention in research [17]. The WPT technologies have been confirmed to be capable of prolonging the lifetime of network devices and sustaining the network [18], [19]. By combining WPT technologies with UAV and applying UAV as an energy supporter, an improved WPT performance can be expected in UAV-enabled WPT networks. In literature, much work [20]–[23] has been done in studying the UAV trajectory design in pure WPT networks. In particular, the work in [20]–[22] has considered a linear energy harvesting (EH) process, which is indeed an approximate model and not practical as shown in [24], [25], since there is a dramatic difference in EH efficiency when the received power changes. More accurately, two models characterizing the non-linearity in EH have been proposed, i.e., a statistic model [25], which is obtained by

curve fitting on statistic data, and an analytical model [26], which is formulated from the structure of conversion circuit. Based on the analytical non-linear model, the optimal structure of a UAV trajectory in pure WPT networks with an omni-directional antenna has been proved to be a successive-hover-fly structure in our previous work [23]. However, it is also observed from [23] that with practical EH setups, the harvested power is largely constricted by the significant attenuation in signal transmission.

On the other hand, operating with a directional antenna has been found to stimulate a significantly amplified antenna gain [27], which can definitely help in improving the WPT gain. Regarding the directional beamforming strategy, there are generally two choices, i.e., digital and analog beamforming. According to [28], [29], analog beamforming has shown a relatively lower flexibility, however, a much lower operation complexity and a low cost compared to the digital directional beamforming. Without channel state information, the authors in [30] have adopted an analog directional antenna and studied a UAV-enabled WPT network with only two users. The applied model is a flat-top model, which approximates the gain in 3dB beamwidth to a constant and is more popular in coverage analysis [31]. In WPT, this inaccurate directional antenna model will result in an unignorable estimation error of the received RF power, and an even larger deviation in evaluating the harvested power due to the varying EH efficiency with respect to the received power. To the best of our knowledge, for a multi-user WPT network assisted by a UAV with the directional antenna, it is still missing in the literature how to efficiently design the UAV trajectory and antenna orientation, especially when considering an accurate pattern model of the directional antenna.

In this work, we consider a UAV-enabled multi-user WPT network, where the UAV operates with a directional antenna utilizing a uniform linear array (ULA) and performing analog beamforming. In addition, an analytical non-linear EH model [26] is taken into account for characterizing the WPT performance. *For the first time*, we consider a joint design, i.e., jointly optimizing the UAV trajectory and directional antenna orientation, aiming at maximizing the minimum harvested energy among all users. By constructing a convex approximation of the focused problem, we address the joint optimization problem with an iterative algorithm which guarantees a convergence behaviour of the WPT performance and eventually results in an efficient suboptimal solution. The main contributions of our work are listed as follows:

- **Modified cosine antenna pattern:** When processing a ULA directional antenna pattern,

the existing models [32] contains a fractional expression where both the numerator and the denominator involve the sine functions, i.e., introducing significant difficulty in analytically designing systems with analog directional beamforming. To tackle the difficulty, we have proposed a modified cosine antenna pattern, based on the existing antenna pattern approximation. The proposed model has kept both accuracy, while the parameter can be adjusted to unlimitedly approach to the existing cosine antenna pattern model, and tractability. This proposed model facilitates not only this work but also other designs under scenarios with analog directional beamforming.

- **Joint design on UAV trajectory and directional antenna orientation:** In literature, all the existing works [33]–[36] regarding a joint design of directional beamforming and UAV trajectory, have performed an alternating optimization strategy. Namely, in these works, beamforming related parameters are optimized with fixed UAV trajectory, while alternately the UAV trajectory is designed based on a fixed beamforming strategy. The separation of optimization variables into two groups makes the problem easier to be solved, but may also weaken the inner connections between the two groups of variables. In our work, we focus on a joint optimization instead. In each iteration of our proposed algorithm, the directional beamforming and UAV trajectory are jointly optimized in a single convex optimization problem. This methodology is highly extensible to different UAV trajectory design problems involving communication with beamforming.
- **Convex approximation:** During our work in constructing a convex approximation of the considered problem, we have proved and adopted a mathematical lemma for approximating a class of univariate functions to convex ones. Following the proved lemma, complex models in optimization problems highly likely become analysable, i.e., can be tightly approximated and corresponding problems can be efficiently solved via similar iterative algorithms as this work.
- **Simulative evaluation:** Via simulations, we evaluate the performance of the proposed joint design. In particular, the tradeoff between the coverage and user harvested power is investigated in terms of UAV height. We learn that a low UAV height is always preferred in maximizing the harvested power of the worst case user. More importantly, although the omni-directional antenna is known to be capable of providing a larger coverage than a directional antenna, our results show that with a relatively high user density in the network,

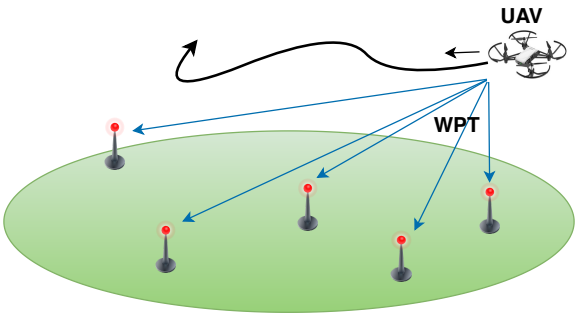

Fig. 1. An example of UAV-enabled WPT networks.

the directional antenna can also overcome the drawback in limited coverage by orienting the beamforming direction to far points and achieve an even better WPT performance than an omni-directional antenna.

The remaining part of the paper is organized as follows. At first, we state the models of the directional antenna gain and non-linear EH and formulate the considered problem in Section II. Then, in Section III, we reformulate the problem based on an approximate model and propose an iterative algorithm solution, which are further numerically evaluated in Section IV. Finally, we conclude our work and make remarks on the possible future extensions in Section V.

II. Preliminary

In this section, we describe our system model and introduce the interested problem.

A. System Model

We study a UAV-enabled wireless sensor network, where multiple sensor nodes (SNs) are distributed on the ground surface, as shown in Fig. 1. We assume that there are K SNs and denote the corresponding horizontal position of SN k by $(w_{x,k}, w_{y,k}), k \in \mathcal{K} \triangleq \{1, 2, \cdots, K\}$. To prolong the lifetimes of these SNs and enrich their battery energy, a single UAV at a fixed altitude H is deployed as an energy supply and responsible for wirelessly transferring energy to the SNs via radio frequency (RF), as displayed in Fig. 1. In addition, SNs' positions are assumed to be a-priori known by the UAV. We consider a fixed time period, $\mathcal{T} \triangleq [0, T]$ with length $T > 0$, for the wireless charging process. Note that the length T of the charging period is pre-designed, perhaps according to the available energy at the UAV or an external time scheduling policy. A larger energy storage at UAV may support a larger charging duration T. Then, at a time point $t \in [0, T]$, the horizontal location of UAV at height H is denoted by $(x(t), y(t))$, which is clearly continuously varying over time t and also continuous over topology. Note that we consider a rotary-wing UAV, which has a high mobility and the speed can be flexibly adjusted [11]. The

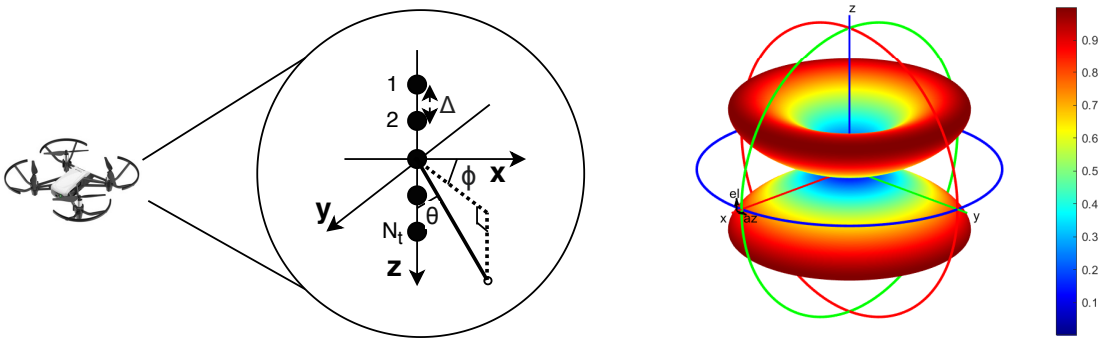

(a) An example of ULA directional antenna ($N_t = 5$). (b) An example of ULA antenna pattern ($N_t = 2$.)

Fig. 2. Figures for directional antenna description.

moving speed of the UAV is constrained by a maximum value V, and the speed constraint is accordingly formulated as $\sqrt{(\dot{x}(t))^2 + (\dot{y}(t))^2} \leq V, \forall t \in \mathcal{T}$, where $\dot{x}(t)$ and $\dot{y}(t)$ are the first-derivatives of $x(t)$ and $y(t)$ in t, respectively.

1) Uniform Linear Array of Directional Antenna: Moreover, the WPT is executed with a directional antenna on the UAV, with which the channel gain can be significantly enhanced in a certain direction. We assume that the applied directional antenna at the UAV is in a manner of a uniform linear array (ULA), where N_t isotropic antenna elements are uniformly placed along a vertical straight line with equal spacing Δ. An example of a ULA directional antenna is shown in Fig. 2(a). As commonly selected in ULA [37], the antenna spacing, i.e., the equal distance between each two neighbour antenna elements, is designed to be half of the wavelength, i.e., $\Delta = \frac{\lambda}{2}$ where λ is the wavelength of the centre carrier frequency for WPT. We focus on an analog directional beamforming, which has already attracted much attentions in diverse applications due to its low cost and low power consumption. We denote by θ_0 the elevation angle of the direction for power concentration in the directional beamforming design of the ULA, namely a maximum power gain will be observed at the direction with elevation angle θ_0. Therefore, the main lobe in the corresponding antenna pattern will be targeted at the direction of the elevation angle θ_0. Then, according to [38], the resulting radiation intensity of the optimal analog beamforming satisfies

$$U(\theta, \phi) \propto \left(\frac{1}{N_t} \frac{\sin(N_t \pi \varphi)}{\sin(\pi \varphi)} \right)^2 \triangleq g_{\mathrm{AP}}(\theta, \phi), \tag{1}$$

where θ and ϕ represent the elevation angle and azimuth angle respectively. $\varphi = \frac{1}{2}(\cos\theta - \cos\theta_0)$ is the auxiliary variable. $g_{\mathrm{AP}}(\theta, \phi)$ is the corresponding antenna pattern, an example of which is provided in Fig. 2(b). According to [37], when the antenna spacing $\Delta = \frac{\lambda}{2}$ and the optimal analog beamforming are applied, the directional antenna gain $g_{\mathrm{A}}(\theta, \phi)$ is expressed by

$$g_{\mathrm{A}}(\theta,\phi)=\frac{U(\theta,\phi)}{\frac{1}{4\pi}\int_0^{2\pi}\int_0^{\pi}U(\theta,\phi)\sin\theta d\theta d\phi}=\frac{1}{N_t}\left(\frac{\sin(N_t\pi\varphi)}{\sin(\pi\varphi)}\right)^2=N_t g_{\mathrm{AP}}(\theta,\phi). \tag{2}$$

Note that as implied in (2) and Fig. 2(b), for a ULA along a straight line, the antenna gain is independent of the azimuth angle ϕ, i.e., the antenna gain can be simplified as $g_{\mathrm{A}}(\theta,\phi)=g_{\mathrm{A}}(\theta)=N_t g_{\mathrm{AP}}(\theta)$. In our considered network, to fully exploit the directional antenna, the elevation angle θ_0, which is the centre of the main lobe, is assumed to be optimized over time, i.e., $\theta_0=\theta_0(t)$. Hence, at time point t, the antenna gain from the UAV for any elevation angle θ is expressed by

$$g_{\mathrm{A}}(\theta,\theta_0(t))=N_t\left(\frac{\sin(N_t\pi\varphi(\theta,\theta_0(t)))}{N_t\sin(\pi\varphi(\theta,\theta_0(t)))}\right)^2\triangleq N_t G_{AP}(\theta,\theta_0(t)), \tag{3}$$

where the auxiliary variable $\varphi(\theta,\theta_0(t))$ also becomes a function in t, i.e., $\varphi(\theta,\theta_0(t))=\frac{1}{2}(\cos\theta-\cos\theta_0(t))$ and $G_{AP}(\theta,\theta_0(t))$ denotes the antenna pattern when the directional antenna is designed for orientation in direction $\theta_0(t)$.

2) Channel Model: Furthermore, in UAV-related wireless communications, the air-to-ground links have a much higher probability to yield LoS and thus, are generally dominated by a LoS component [3]. Therefore, as broadly performed, we adopt a free-space channel model, i.e., the path loss exponent is fixed to be 2, for all channels between the UAV and all SNs. At a time point $t\in\mathcal{T}$, the channel power gain from UAV to an SN k is represented by

$$g_{\mathrm{ch},k}(t)=\frac{\beta_0 N_t G_{AP}(\theta_k(t),\theta_0(t))}{(d_k(t))^2}, \tag{4}$$

where β_0 denotes the channel power gain at a reference distance of unit meter with an isotropic antenna, $d_k(t)$ is the distance from UAV to SN k at time t, i.e.,

$$d_k(t)=\sqrt{(x(t)-w_{x,k})^2+(y(t)-w_{y,k})^2+H^2}, \tag{5}$$

and $\theta_k(t)\in[0,\frac{\pi}{2})$ is the elevation angle of the SN k with respect to the UAV at time t. In particular, we have

$$\cos(\theta_k(t))=\frac{H}{d_k(t)},\ \text{i.e., } \theta_k(t)=\arccos\left(\frac{H}{d_k(t)}\right). \tag{6}$$

Denote by P the constant transmit power of UAV for WPT. Then, the received RF power of SN k at time t is obtained by

$$Q_k(t)=g_{\mathrm{ch},k}(t)P=\frac{\beta_0 P N_t G_{\mathrm{AP}}(\theta_k(t),\theta_0(t))}{(d_k(t))^2}. \tag{7}$$

3) Nonlinear Energy Harvesting: During energy harvesting procedure, the received RF signal will be at first converted into a direct-current (DC) signal and then harvested into the battery set at SNs. The conversion is clearly a non-linear process [24], and thus makes the existing works

[20]–[22], which considered a simplified linear EH models, inaccurate and unrealistic. Due to the significant attenuation of signal in wireless transmission and relatively large distance between UAV and SNs, the received RF signal has a generally small power, which motivates us to adopt a small signal model [39] to process the non-linearity of rectifier (diode) during DC conversion at SNs. As shown in [39], the relation between the voltage v_d and the current $I_{\rm out}$ over a diode can be modelled as $I_{\rm out} = I_s(e^{\frac{v_d}{nv_t}} - 1)$, where the constants n, v_t and I_s respectively denote the ideality factor, the thermal voltage and the reverse bias saturation current at diode. According to [26], by performing a Taylor expansion on the non-linear current function over voltage in diode, the output current $I_{\rm out}$ for harvesting can be characterized by a non-linear implicit function $I_{\rm out}(Q)$ with respect to the received RF power Q. More specifically, as displayed in Eq.(6) in [26], we have

$$e^{\frac{R_{\rm L} I_{\rm out}(Q)}{nv_t}} (I_{\rm out}(Q) + I_{\rm s}) \approx \sum\nolimits_{j=0}^{n'_o} \alpha_j Q^j, \tag{8}$$

where R_L is the load resistance. Notice that the positive truncation order n'_o can become a sufficiently large integer which represents a more accurate non-linear expression of the model. In addition, all the factors α_j are obtained from the Taylor expansion and are definitely positive. Note that with any given Q, the value of $I_{\rm out}(Q)$ can be uniquely determined by solving the equation in (8). Although $I_{\rm out}(Q)$ is an implicit function and cannot be expressed in terms of elementary functions, we can still find an explicit expression for $I_{\rm out}(Q)$ with the assistance of Lambert W function, namely,

$$I_{\rm out}(Q) \approx \frac{nv_t}{R_{\rm L}} W_0 \left(\frac{R_{\rm L}}{nv_t} e^{\frac{R_{\rm L} I_s}{nv_t}} \sum\nolimits_{j=0}^{n'_o} \alpha_j Q^j \right) - I_{\rm s}, \tag{9}$$

where W_0 is the principle branch of Lambert W function, which is the inverse relation of function $f(x) = xe^x$. Afterwards, the charged (harvested) power $P_{\rm ch}$ can be directly expressed by the output current $I_{\rm out}(Q)$, i.e., $P_{\rm ch} = \left(I_{\rm out}(Q)\right)^2 R_L$, which implies that the charged power $P_{\rm ch}$ is also an implicit nonlinear function of received RF power Q, denoted by $\mathcal{F}_{\rm nl}(Q)$.

Therefore, at time t, the harvested power $P_{{\rm ch},k}(t)$ at SN k is denoted by

$$P_{{\rm ch},k}(t) = \mathcal{F}_{\rm nl}(Q_k(t)) \triangleq \left(I_{\rm out}(Q_k(t))\right)^2 R_L. \tag{10}$$

Convexity in nonlinear EH model: Although the charged power $P_{{\rm ch},k}(t)$ cannot be derived in terms of elementary functions, we can apply the convexity of this non-linear process in $\mathcal{F}_{\rm nl}$, which has been already proved in [26]. In particular, let $u(t) = \frac{\beta_0 P N_t}{Q_k(t)} = \frac{(d_k(t))^2}{G_{AP}(\theta_k(t),\theta_0(t))}$, and $Q_k(t)$ described in (7) can be reformulated as $Q_k(t) = Q_k^*(u) = \frac{\beta_0 P N_t}{u}$. Then, the first-order

and second-order derivatives of $Q_k^*(u)$ are given by $\dot{Q^*}_k(u) = -\frac{\beta_0 P N_t}{u^2}$ and $\ddot{Q^*}_k(u) = \frac{2\beta_0 P N_t}{u^3}$, respectively. Therefore, the following inequality can be proved to hold

$$\ddot{Q^*}_k(u)Q_k^*(u) - \left(\dot{Q^*}_k(u)\right)^2 = \left(\frac{2\beta_0 P N_t}{u^3}\right) \cdot \frac{\beta_0 P N_t}{u} - \left(-\frac{\beta_0 P N_t}{u^2}\right)^2 = \frac{\beta_0^2 P^2 N_t^2}{u^4} > 0. \quad (11)$$

According to [26], satisfying the condition $\ddot{Q^*}_k(u)Q_k^*(u) - \left(\dot{Q^*}_k(u)\right)^2 \geq 0$ definitely makes the function $\mathcal{F}_{\text{nl}}(Q_k(t)) = \mathcal{F}_{\text{nl}}(Q_k^*(u))$ be convex with respect to u. In other words, for our considered network, $P_{\text{ch},k}(t) = \mathcal{F}_{\text{nl}}(Q_k(t))$ is convex in $\frac{(d_k(t))^2}{G_{AP}(\theta_k(t),\theta_0(t))}$, which facilitates us in analytically modeling and optimizing the network performance.

B. Problem Statement

To fully deploy the WPT UAV and to improve the energy harvesting behaviour, all SNs can simultaneously accept the wirelessly transferred power for energy harvesting during the whole charging period $\mathcal{T}$. As a result, the total harvested energy at SN k is given by

$$E_k(\{x(t), y(t), \theta(t)\}) = \int_0^T P_{ch,k}(t)dt = \int_0^T \mathcal{F}_{\text{nl}}(Q_k(t))dt, \quad (12)$$

where $Q_k(t)$ is given in (7) and is actually a function of $x(t)$, $y(t)$ and $\theta_0(t)$. While taking the fairness among SNs into account and focusing on enhancing the WPT performance, we aim at jointly designing the UAV trajectory $\{x(t), y(t)\}$ and the directional antenna orientation $\theta_0(t)$ to maximize the minimal harvested energy among all SNs during the charging period $\mathcal{T}$. Thus, the considered optimization problem can be formulated as

$$(\text{OP}): \max_{\{x(t),y(t),\theta_0(t)\}} \min_{k\in\mathcal{K}} E_k(\{x(t), y(t), \theta_0(t)\}) \quad (13a)$$

$$\text{s.t.} \quad \sqrt{\left(\dot{x}(t)\right)^2 + \left(\dot{y}(t)\right)^2} \leq V, \forall t \in \mathcal{T}, \quad (13b)$$

$$0 \leq \theta_0(t) < \frac{\pi}{2}, \forall t \in \mathcal{T}. \quad (13c)$$

Since it makes no benefits to orient the directional antenna on UAV to the above directions, the elevation angle for orientation $\theta_0(t)$ is constricted in interval $[0, \frac{\pi}{2})$, as indicated in the constraint (13c) in the problem (OP). Next, with assistance of the auxiliary variable E, the original problem (OP) is equivalently reformulated as

$$(\text{P1}): \max_{\{x(t),y(t),\theta_0(t)\},E} E \quad (14a)$$

$$\text{s.t.} \quad E_k(\{x(t), y(t), \theta_0(t)\}) \geq E, \forall k \in \mathcal{K}. \quad (14b)$$

$$\sqrt{\left(\dot{x}(t)\right)^2 + \left(\dot{y}(t)\right)^2} \leq V, \forall t \in \mathcal{T}, \quad (14c)$$

$$0 \leq \theta_0(t) < \frac{\pi}{2}, \forall t \in \mathcal{T}. \quad (14d)$$

It should be pointed out that both the problems (OP) and (P1) have contained infinite variables $\{x(t), y(t), \theta_0(t)\}$, as the time scale t is continuous, which makes the problem exceedingly complicated to be addressed. Besides, the complex implicit non-linear function $\mathcal{F}_{nl}$ and the multi-modal function of antenna gain in (3) make a concavity property of function $E_k(\{x(t), y(t), \theta_0(t)\})$ inaccessible, so that both problems (OP) and (P1) are not convex and cannot be efficiently optimally solved via convex optimization techniques. Therefore, in order to address the difficulties and to obtain a jointly optimized UAV trajectory and directional orientation scheme, we apply some appropriate approximations and reformulate the problem in the next section. Subsequently, based on the reformulated problem, an iterative algorithm for the solution will be proposed.

III. Proposed Joint Optimization Algorithm

To facilitate the problem analysis, in this section, we first reformulate the problem (P1) via quantizing the UAV trajectory in the time domain and tightly approximating the antenna pattern model for antenna gain. Afterwards, a tight convex approximation for the reformulated problem will be further constructed, with which the problem will be iteratively solved via efficiently handling a convex optimization problem in each iteration. The iterative algorithm and the corresponding feasible point initialization are provided at the end of the section.

A. Problem Reformulation

1) Time Quantization on UAV Trajectory: Note that the continuity of time t in interval $[0, T]$ introduces infinite number of variables in the problem (P1), which makes the problem extremely difficult to be analytically solved. We address this issue by uniformly dividing the interval into N time slots with equal lengths $dT = \frac{T}{N}$. Note that the length of each time slot dT is sufficiently small so that in each time slot the position of UAV can be assumed to be static and the directional antenna orientation can be considered to be constant. Hence, when the resolution of the time quantization dT approaches to zero, this approximation will be more accurate, i.e., making the UAV trajectory/path become smoother. On the other hand, a small dT also leads to a large number N of time slots. In other words, the choice of resolution dT actually directly influences the tradeoff between the approximation accuracy and the problem complexity (in terms of the number of variables required to be optimized).

In addition, in time slot $n \in \mathcal{N} \triangleq \{1, ..., N\}$, we denote the static position of UAV and the static directional antenna orientation by $(x[n], y[n])$ and $\theta_0[n]$. Then, the UAV speed constraint

becomes

$$(x[n+1]-x[n])^2+(y[n+1]-y[n])^2 \leq V^2dT^2,\ \forall n \in \mathcal{N},\ n \neq N, \tag{15}$$

which representing that the distance between UAV positions in each two neighbour time slots should be constricted by the maximum movement VdT within a time slot.

2) Antenna Pattern Approximation: The antenna pattern given in (3) has sine functions in both the numerator and denominator, and is thus multimodal and not tractable in performance analysis [32]. Therefore, an approximation of the directional antenna pattern with both accuracy and tractability is highly recommended. For this purpose, the authors in [32] have proposed a cosine antenna pattern approximation, as shown in Fig. 3, in which the main lobe in antenna pattern is represented by a square of cosine function while the remaining side lobes are ignored. In our considered problem, the charged power $P_{\text{ch},k}(t)$ has been proved to be convex in $\frac{(d_k(t))^2}{G_{\text{A}}(\theta_k(t),\theta_0(t))}$ which goes to infinity with a zero antenna gain. In other words, the approximation in [32] cannot be directly applied in this work. To deploy the convexity and facilitate the system analysis, we are motivated to propose a modified cosine antenna pattern approximation considering both the main lobe and side lobes in antenna pattern:

$$\begin{aligned} G_{\text{AP-mc}}(\theta_k(t),\theta_0(t)) &= \mathcal{F}_{\text{A}}(\varphi(\theta_k(t),\theta_0(t))) \\ &= \begin{cases} \cos^2\left(\frac{N_t\pi}{2}\varphi(\theta_k(t),\theta_0(t))\right), & |\varphi(\theta_k(t),\theta_0(t))| < \frac{\delta}{N_t}, \\ \frac{\cos^2(\frac{\delta\pi}{2})}{\sqrt{2N_t\pi\tan(\frac{\delta\pi}{2})(|\varphi(\theta_k(t)-\theta_0(t))|-\frac{\delta}{N_t})+1}}, & |\varphi(\theta_k(t),\theta_0(t))| \geq \frac{\delta}{N_t}, \end{cases} \end{aligned} \tag{16}$$

where $\delta \in (0,1)$ is the modification factor. The introduction of δ makes that the modified cosine antenna pattern can have an extremely small value but always be positive. Distinctly, when δ goes to 1, the modified cosine antenna pattern approaches to the proposed cosine pattern in [32], as implied in Fig. 3. It is worthwhile to mention that function $\mathcal{F}_{\text{A}}$, i.e., representing the relationship between the modified pattern model $G_{\text{AP-mc}}(\theta_k(t),\theta_0(t))$ and $\varphi(\theta_k(t),\theta_0(t))$, is a continuous function, as displayed in (16). By adopting the modified cosine antenna pattern $G_{\text{AP-mc}}(\theta_k(t),\theta_0(t))$, the antenna gain in time slot n can be further given by

$$G_{\text{A-mc}}(\theta_k[n],\theta_0[n]) = N_tG_{\text{AP-mc}}(\theta_k[n],\theta_0[n]) = N_t\mathcal{F}_{\text{A}}(\varphi_k[n]), \tag{17}$$

where $\theta_k[n]$ represents the elevation angle of SN k to the UAV in time slot n and is given by

$$\theta_k[n] = \arccos\left(\frac{H}{d_k[n]}\right), d_k[n] = \sqrt{(x[n]-w_{x,k})^2+(y[n]-w_{y,k})^2+H^2}. \tag{18}$$

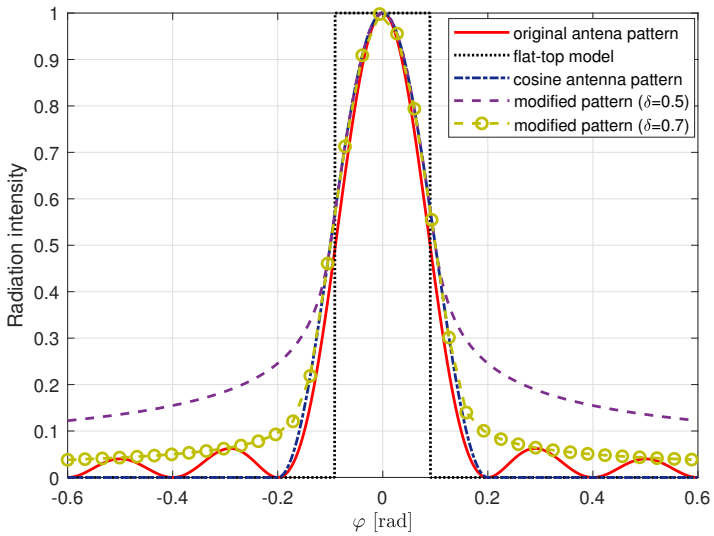

Fig. 3. Comparison of different antenna pattern approximation ($N_t = 5$).

Accordingly, we have the auxiliary variable $\varphi_k[n] = \varphi(\theta_k[n], \theta_0[n]) = \frac{1}{2}(\frac{H}{d_k[n]} - \cos\theta_0[n])$. Since the variable $\theta_0[n]$ for directional antenna orientation only appears in $\varphi_k[n]$ within a term of $\cos\theta_0[n]$, we substitute the variables $\theta_0[n]$ with a new variable $\mu[n] = \cos\theta_0[n] \in (0, 1]$ for simplification and reformulate $\varphi_k[n]$ as

$$\varphi_k[n] = \frac{1}{2}(\frac{H}{d_k[n]} - \mu[n]). \tag{19}$$

As a result, the accumulated harvested energy at SN k within all N time slots are denoted by

$$E_k(\{x[n], y[n], \mu[n]\}) = \sum_{n=1}^{N} \mathcal{F}_{nl}\left(\frac{\beta_0 P N_t \mathcal{F}_{\mathrm{A}}(\varphi_k[n])}{d_k[n]^2}\right) dT. \tag{20}$$

3) Reformulated Problem: With the time-slot division on the trajectory and modified cosine antenna pattern, the problem (P1) is finally approximately reformulated as

$$(\mathrm{P2}): \max_{\{x[n],y[n],\mu[n]\},E} \quad E \tag{21a}$$

$$\text{s.t.} \quad \sum_{n=1}^{N} \mathcal{F}_{nl}\left(\frac{\beta_0 P N_t \mathcal{F}_{\mathrm{A}}(\varphi_k[n])}{d_k[n]^2}\right) dT \geq E, \ \forall k \in \mathcal{K}, \tag{21b}$$

$$(x[n+1]-x[n])^2+(y[n+1]-y[n])^2 \leq V^2 dT^2, \ \forall n \in \mathcal{N}, n \neq N, \tag{21c}$$

$$0 < \mu[n] \leq 1, \ \forall n \in \mathcal{N}, \tag{21d}$$

where the expressions of $\mathcal{F}_{\mathrm{A}}(\varphi)$, $d_k[n]$ and $\varphi_k[n]$ are given in (16), (18) and (19), respectively.

Note that the constraint given in (21b) is not convex due to the non-concavity of function $\mathcal{F}_{nl}\left(\frac{\beta_0 P N_t \mathcal{F}_{\mathrm{A}}(\varphi_k[n])}{d_k[n]^2}\right)$. Thus, the reformulated problem (P2) is still not convex and cannot be directly optimally solved. In the next subsection, we perform a tight convex approximation on

the problem, which help us to efficiently solve the problem in an iterative manner.

B. Convex Approximation

In the problem (P2), the objective is apparently affine and the constraints except (21b) can be simply proved to be convex. Thus, to construct a convex approximation of problem (P2), we are supposed to approximate the constraint (21b) to a convex one, namely to find a concave function $P_{k,n}^{(r)}$ for the harvested power $\mathcal{F}_{nl}\left(\frac{\beta_0 P N_t \mathcal{F}_{\mathrm{A}}(\varphi_k[n])}{d_k[n]^2}\right)$, so that $\mathcal{F}_{nl}\left(\frac{\beta_0 P N_t \mathcal{F}_{\mathrm{A}}(\varphi_k[n])}{d_k[n]^2}\right) \geq P_{k,n}^{(r)}(x[n], y[n], \mu[n])$ and the equality holds at a local point $(x^{(r)}[n], y^{(r)}[n], \mu^{(r)}[n])$.

Recall that as discussed in Section II, the function $\mathcal{F}_{\mathrm{nl}}\left(\frac{\beta_0 P N_t \mathcal{F}_{\mathrm{A}}(\varphi_k[n])}{d_k[n]^2}\right)$ is convex with respect to $\frac{d_k[n]^2}{\mathcal{F}_{\mathrm{A}}(\varphi_k[n])}$. Based on the property of convex functions, for any pair of k and n, we can obtain an inequality

$$\mathcal{F}_{\mathrm{nl}}\left(\frac{\beta_0 P N_t \mathcal{F}_{\mathrm{A}}(\varphi_k[n])}{d_k[n]^2}\right) \geq -A_{1,k,n}^{(r)}\left(\frac{d_k[n]^2}{\mathcal{F}_{\mathrm{A}}(\varphi_k[n])}\right) + A_{2,k,n}^{(r)}, \tag{22}$$

where the constants $A_{1,k,n}^{(r)}$ and $A_{2,k,n}^{(r)}$ are given by

$$A_{1,k,n}^{(r)} = \mathcal{F}'_{nl}\left(\frac{\beta_0 P N_t \mathcal{F}_{\mathrm{A}}(\varphi_k^{(r)}[n])}{d_k^{(r)}[n]^2}\right) \frac{\beta_0 P N_t d_k^{(r)}[n]^4}{\left(\mathcal{F}_{\mathrm{A}}(\varphi_k^{(r)}[n])\right)^2}, \tag{23}$$

$$A_{2,k,n}^{(r)} = \mathcal{F}_{nl}\left(\frac{\beta_0 P N_t \mathcal{F}_{\mathrm{A}}(\varphi_k^{(r)}[n])}{d_k^{(r)}[n]^2}\right) + A_{1,k,n}^{(r)}\left(\frac{d_k^{(r)}[n]^2}{\mathcal{F}_{\mathrm{A}}(\varphi_k^{(r)}[n])}\right), \tag{24}$$

and the terms $d_k^{(r)}[n]$ and $\varphi_k^{(r)}[n]$ are respectively the obtained values of $d_k[n]$ and $\varphi_k[n]$ at local point $(x^{(r)}[n], y^{(r)}[n], \mu^{(r)}[n])$. Note that $-A_{1,k,n}^{(r)}$ is the first derivative of $\mathcal{F}_{\mathrm{nl}}\left(\frac{\beta_0 P N_t \mathcal{F}_{\mathrm{A}}(\varphi_k[n])}{d_k[n]^2}\right)$ to $\frac{d_k[n]^2}{\mathcal{F}_{\mathrm{A}}(\varphi_k[n])}$ at local point $(x^{(r)}[n], y^{(r)}[n], \mu^{(r)}[n])$. Clearly, the equality in (22) holds at the local point during the Taylor expansion. Moreover, as more received power at an SN always leads to a larger converted power for energy harvesting, the non-linear function $\mathcal{F}_{\mathrm{nl}}$ is clearly an increasing function, i.e., constants $A_{1,k,n}^{(r)}$ and $A_{2,k,n}^{(r)}$ are both positive.

Then, due to the non-convexity of function $\frac{d_k[n]^2}{\mathcal{F}_{\mathrm{A}}(\varphi_k[n])}$, we are motivated to perform a further convex approximation to (22). It should be mentioned that with the modified cosine antenna pattern in (16), the function $\mathcal{F}_{\mathrm{A}}(\varphi_k[n])$ is guaranteed to be positive. According to the inequality of arithmetic and geometric means, i.e., $ab \leq \frac{1}{2}a^2 + \frac{1}{2}b^2$ holds $\forall a, b \in \mathcal{R}^+$ and the equality holds when $a = b$, we can obtain from (22)

$$
\begin{aligned}
\mathcal{F}_{\text{nl}}\left(\frac{\beta_0 P N_t \mathcal{F}_{\text{A}}(\varphi_k[n])}{d_k[n]^2}\right) \;&\geq\; -A_{1,k,n}^{(r)}\left(\frac{d_k[n]^2}{\mathcal{F}_{\text{A}}(\varphi_k[n])}\right) + A_{2,k,n}^{(r)} \\
&= -A_{1,k,n}^{(r)}\frac{1}{F_{1,k,n}^{(r)}}\underline{F_{1,k,n}^{(r)} d_k[n]^2}\cdot\underline{\frac{1}{\mathcal{F}_{\text{A}}(\varphi_k[n])}} + A_{2,k,n}^{(r)} \\
&\geq -A_{1,k,n}^{(r)}\frac{1}{F_{1,k,n}^{(r)}}\underline{\frac{1}{2}\left(F_{1,k,n}^{(r)} d_k[n]^2\right)^2} - A_{1,k,n}^{(r)}\frac{1}{F_{1,k,n}^{(r)}}\underline{\frac{1}{2\left(\mathcal{F}_{\text{A}}(\varphi_k[n])\right)^2}} + A_{2,k,n}^{(r)} \\
&= -A_{1,k,n}^{(r)}\frac{F_{1,k,n}^{(r)} d_k[n]^4}{2} - A_{1,k,n}^{(r)}\frac{1}{2F_{1,k,n}^{(r)}\left(\mathcal{F}_{\text{A}}(\varphi_k[n])\right)^2} + A_{2,k,n}^{(r)},
\end{aligned} \tag{25}
$$

where the terms with underlines are respectively representing the terms a and b in applied inequality and the positive constant $F_{1,k,n}^{(r)}$ is given by

$$
F_{1,k,n}^{(r)} = \frac{1}{\mathcal{F}_{\text{A}}(\varphi_k^{(r)}[n])}\frac{1}{d_k^{(r)}[n]^2}, \tag{26}
$$

which assures that the equality in (25) holds at the local point $(x^{(r)}[n], y^{(r)}[n], \mu^{(r)}[n])$.

Note that by observing the approximation results in (25), we find that the concave approximation $P_{k,n}^{(r)}$ can be completed when a tight upper-bound convex approximation of $\frac{1}{(\mathcal{F}_{\text{A}}(\varphi_k[n]))^2}$ can be obtained. Towards this end, we first introduce a mathematical lemma, i.e., Lemma 1, to facilitate the following approximations.

Lemma 1. *For any continuous function $h(\gamma)$ ($\gamma \in \mathcal{D}$), where $\mathcal{D}$ is a continuous domain, and a given value $\gamma_0 \in \mathcal{D}$, if the first-order derivative of $h(\gamma)$ is continuous and the second-order derivative $h''(\gamma) \leq c$ ($c \geq 0$), then we have the following inequality holds that*

$$
h(\gamma) \leq \frac{c}{2}\gamma^2 + (h'(\gamma_0) - c\gamma_0)\gamma + h(\gamma_0) - \gamma_0 h'(\gamma_0) + \frac{c}{2}\gamma_0^2,\ \forall \gamma \in \mathcal{D}, \tag{27}
$$

and the equality holds when $\gamma = \gamma_0$.

Proof. The proof is provided in Appendix A. □

Then, we focus on the function $\frac{1}{(\mathcal{F}_{\text{A}}(\varphi_k[n]))^2}$. According to the definition in (16), we have

$$
\frac{1}{\left(\mathcal{F}_{\text{A}}(\varphi_k[n])\right)^2} = \begin{cases} \frac{1}{\cos^4(\frac{N_t\pi}{2}\varphi_k[n])}, & |\varphi_k[n]| < \frac{\delta}{N_t}, \\ \frac{2N_t\pi\tan(\frac{\delta\pi}{2})(|\varphi_k[n]| - \frac{\delta}{N_t}) + 1}{\cos^4(\frac{\delta\pi}{2})}, & |\varphi_k[n]| \geq \frac{\delta}{N_t}. \end{cases} \tag{28}
$$

Function $\frac{1}{(\mathcal{F}_{\text{A}}(\varphi_k[n]))^2}$ is clearly continuous, and its first derivative to $\varphi_k[n]$ is given by

$$\left(\frac{1}{\left(\mathcal{F}_{\mathrm{A}}(\varphi_k[n])\right)^2}\right)'_{\varphi_k[n]} = \frac{-2\mathcal{F}'_{\mathrm{A}}(\varphi_k[n])}{\left(\mathcal{F}_{\mathrm{A}}(\varphi_k[n])\right)^3} = \begin{cases} \frac{2N_t\pi\sin(\frac{N_t\pi}{2}\varphi_k[n])}{\cos^5(\frac{N_t\pi}{2}\varphi_k[n])}, & |\varphi_k[n]| < \frac{\delta}{N_t}, \\ \frac{2N_t\pi\sin(\frac{\delta\pi}{2})}{\cos^5(\frac{\delta\pi}{2})}, & \varphi_k[n] \geq \frac{\delta}{N_t}, \\ -\frac{2N_t\pi\sin(\frac{\delta\pi}{2})}{\cos^5(\frac{\delta\pi}{2})}, & \varphi_k[n] \leq -\frac{\delta}{N_t}, \end{cases} \tag{29}$$

which is apparently continuous. The second-order derivative of $\frac{1}{\left(\mathcal{F}_{\mathrm{A}}(\varphi_k[n])\right)^2}$ to $\varphi_k[n]$ is

$$\left(\frac{1}{\left(\mathcal{F}_{\mathrm{A}}(\varphi_k[n])\right)^2}\right)''_{\varphi_k[n]} = \begin{cases} \frac{N_t^2\pi^2+4N_t^2\pi^2\sin^2(\frac{N_t\pi}{2}\varphi_k[n])}{\cos^4(\frac{N_t\pi}{2}\varphi_k[n])}, & |\varphi_k[n]| < \frac{\delta}{N_t}, \\ 0, & |\varphi_k[n]| > \frac{\delta}{N_t}. \end{cases} \tag{30}$$

Note that the second-order derivative does not exist when $|\varphi_k[n]| = \frac{\delta}{N_t}$. Thus, from the above expression, we have $\left(\frac{1}{\left(\mathcal{F}_{\mathrm{A}}(\varphi_k[n])\right)^2}\right)''_{\varphi_k[n]} < \frac{5N_t^2\pi^2}{\cos^4(\frac{\delta\pi}{2})}$. According to Lemma 1, we can obtain that

$$\frac{1}{\left(\mathcal{F}_{\mathrm{A}}(\varphi_k[n])\right)^2} \leq B^{(r)}_{1,k,n}(\varphi_k[n])^2 + B^{(r)}_{2,k,n}(\varphi_k[n]) + B^{(r)}_{3,k,n}, \tag{31}$$

where the constants $B^{(r)}_{1,k,n}$, $B^{(r)}_{2,k,n}$ and $B^{(r)}_{3,k,n}$ are formulated as

$$B^{(r)}_{1,k,n} = \frac{5N_t^2\pi^2}{2\cos^4(\frac{\delta\pi}{2})} > 0, \tag{32}$$

$$B^{(r)}_{2,k,n} = \frac{-2\mathcal{F}'_{\mathrm{A}}(\varphi_k^{(r)}[n])}{\left(\mathcal{F}_{\mathrm{A}}(\varphi_k^{(r)}[n])\right)^3} - \frac{5N_t^2\pi^2}{\cos^4(\frac{\delta\pi}{2})}\varphi_k^{(r)}[n], \tag{33}$$

$$B^{(r)}_{3,k,n} = \frac{1}{\left(\mathcal{F}_{\mathrm{A}}(\varphi_k^{(r)}[n])\right)^2} + \frac{2\mathcal{F}'_{\mathrm{A}}(\varphi_k^{(r)}[n])\varphi_k^{(r)}[n]}{\left(\mathcal{F}_{\mathrm{A}}(\varphi_k^{(r)}[n])\right)^3} + \frac{5N_t^2\pi^2}{2\cos^4(\frac{\delta\pi}{2})}(\varphi_k^{(r)}[n])^2. \tag{34}$$

By combining the definition of $\varphi_k[n]$ in (19) with the approximation in (31), we have

$$\begin{aligned} \frac{1}{\left(\mathcal{F}_{\mathrm{A}}(\varphi_k[n])\right)^2} &\leq \frac{B^{(r)}_{1,k,n}}{4}(\frac{H}{d_k[n]} - \mu[n])^2 + \frac{B^{(r)}_{2,k,n}}{2}\left(\frac{H}{d_k[n]} - \mu[n]\right) + B^{(r)}_{3,k,n} \\ &= \frac{B^{(r)}_{1,k,n}}{4}\frac{H^2}{d_k[n]^2} + \left(\frac{B^{(r)}_{2,k,n}}{2} - \frac{3B^{(r)}_{1,k,n}}{4}\right)\frac{H}{d_k[n]} + \frac{B^{(r)}_{1,k,n}}{4}(3-2\mu[n])\frac{H}{d_k[n]} \\ &\quad + \frac{B^{(r)}_{1,k,n}}{4}\mu[n]^2 - \frac{B^{(r)}_{2,k,n}}{2}\mu[n] + B^{(r)}_{3,k,n}. \end{aligned} \tag{35}$$

Note that $B^{(r)}_{1,k,n} > 0$ and that $\mu[n] \in (0,1]$ makes $3 - 2\mu[n] > 0$ hold. Therefore, by defining a positive constant $F^{(r)}_{2,k,n} = \frac{H}{d_k^{(r)}[n]} \cdot \frac{1}{3-2\mu^{(r)}[n]} > 0$, based on the inequality of arithmetic and geometric means, we have

$$\begin{aligned}
\frac{1}{\left(\mathcal{F}_{\mathrm{A}}(\varphi_k[n])\right)^2} &\leq \frac{B_{1,k,n}^{(r)}}{4}\frac{H^2}{d_k[n]^2}+\left(\frac{B_{2,k,n}^{(r)}}{2}-\frac{3B_{1,k,n}^{(r)}}{4}\right)\frac{H}{d_k[n]}+\frac{B_{1,k,n}^{(r)}}{4F_{2,k,n}^{(r)}}\underline{\underline{F_{2,k,n}^{(r)}(3-2\mu[n])}}\cdot\underline{\underline{\frac{H}{d_k[n]}}} \\
&\quad +\frac{B_{1,k,n}^{(r)}}{4}\mu[n]^2-\frac{B_{2,k,n}^{(r)}}{2}\mu[n]+B_{3,k,n}^{(r)}. \qquad (36a)\\
&\leq \underbrace{\frac{B_{1,k,n}^{(r)}}{4}\frac{H^2}{d_k[n]^2}+\left(\frac{B_{2,k,n}^{(r)}}{2}-\frac{3B_{1,k,n}^{(r)}}{4}\right)\frac{H}{d_k[n]}+\frac{B_{1,k,n}^{(r)}}{4F_{2,k,n}^{(r)}}\underline{\underline{\frac{H^2}{2d_k[n]^2}}}}_{h_{1,k,n}^{(r)}(d_k[n])} \\
&\quad +\underbrace{\frac{B_{1,k,n}^{(r)}}{4F_{2,k,n}^{(r)}}\underline{\underline{\frac{\left(F_{2,k,n}^{(r)}(3-2\mu[n])\right)^2}{2}}}+\frac{B_{1,k,n}^{(r)}}{4}\mu[n]^2-\frac{B_{2,k,n}^{(r)}}{2}\mu[n]+B_{3,k,n}^{(r)}}_{h_{2,k,n}^{(r)}(\mu[n])} \qquad (36b)\\
&\triangleq h_{1,k,n}^{(r)}(d_k[n])+h_{2,k,n}^{(r)}(\mu[n]), \qquad (36c)
\end{aligned}$$

where the equality also holds at the local point $(x^{(r)}[n], y^{(r)}[n], \mu^{(r)}[n])$ with the assistance of $F_{2,k,n}^{(r)}$. Clearly, the function $h_{2,k,n}^{(r)}(\mu[n])$ is convex in $\mu[n]$, while $h_{1,k,n}^{(r)}(d_k[n])$ is convex in $d_k[n]$ however not jointly convex in $x[n]$ and $y[n]$ according to (18). Therefore, we next focus on the function $h_{1,k,n}^{(r)}(d_k[n])$, which can be reformulated as

$$h_{1,k,n}^{(r)}(d_k[n])=\frac{B_{1,k,n}^{(r)}}{4}\left(1+\frac{1}{2F_{2,k,n}^{(r)}}\right)\frac{H^2}{d_k[n]^2}+\left(\frac{B_{2,k,n}^{(r)}}{2}-\frac{3B_{1,k,n}^{(r)}}{4}\right)\frac{H}{d_k[n]}. \qquad (37)$$

Then, we treat the term $(x[n]-w_{x,k})^2+(y[n]-w_{y,k})^2$ in $h_{1,k,n}^{(r)}$ as a variable γ, and consider a function $h_0(\gamma)=\frac{B_{1,k,n}^{(r)}}{4}\left(1+\frac{1}{2F_{2,k,n}^{(r)}}\right)\frac{H^2}{\gamma+H^2}+\left(\frac{B_{2,k,n}^{(r)}}{2}-\frac{3B_{1,k,n}^{(r)}}{4}\right)\frac{H}{\sqrt{\gamma+H^2}}$ $(\gamma\geq 0)$, which is second-order differentiable. With a single variable γ, it can be easily proved that the second-order derivative of $h_0(\gamma)$ satisfies

$$\begin{aligned}
h_0''(\gamma) &= \frac{B_{1,k,n}^{(r)}}{4}\left(1+\frac{1}{2F_{2,k,n}^{(r)}}\right)\frac{2H^2}{(\gamma+H^2)^3}+\left(\frac{B_{2,k,n}^{(r)}}{2}-\frac{3B_{1,k,n}^{(r)}}{4}\right)\frac{3H}{4(\sqrt{\gamma+H^2})^5} \\
&\leq \frac{B_{1,k,n}^{(r)}}{4}\left(1+\frac{1}{2F_{2,k,n}^{(r)}}\right)\frac{2}{H^4}+\left|\frac{B_{2,k,n}^{(r)}}{2}-\frac{3B_{1,k,n}^{(r)}}{4}\right|\frac{3}{4H^4}\triangleq C_{1,k,n}^{(r)},\ \forall\gamma\geq 0. \qquad (38)
\end{aligned}$$

Since $C_{1,k,n}^{(r)}>0$, according to Lemma 1, we can get

$$\begin{aligned}
& h_{1,k,n}^{(r)}(d_k[n]) = h_0((x[n]-w_{x,k})^2+(y[n]-w_{y,k})^2) \\
\leq\ & \frac{C_{1,k,n}^{(r)}}{2}((x[n]-w_{x,k})^2+(y[n]-w_{y,k})^2)^2+C_{2,k,n}^{(r)}((x[n]-w_{x,k})^2+(y[n]-w_{y,k})^2)+C_{3,k,n}^{(r)} \\
\triangleq\ & h_{3,k,n}^{(r)}(x[n],y[n]), \qquad (39)
\end{aligned}$$

where $C_{2,k,n}^{(r)}$ and $C_{3,k,n}^{(r)}$ are obtained as based on Lemma 1

$$C_{2,k,n}^{(r)} = h_0'(\gamma_0^{(r)}) - C_{1,k,n}^{(r)}\gamma_0^{(r)}, \tag{40}$$

$$C_{3,k,n}^{(r)} = h_0(\gamma_0^{(r)}) - \frac{C_{1,k,n}^{(r)}}{2}(\gamma_0^{(r)})^2 - C_{2,k,n}^{(r)}\gamma_0^{(r)}, \tag{41}$$

$$\gamma_0^{(r)} = (x^{(r)}[n]-w_{x,k})^2+(y^{(r)}[n]-w_{y,k})^2. \tag{42}$$

For function $h_{3,k,n}^{(r)}(x[n],y[n])$, different sign of the constant $C_{2,k,n}^{(r)}$ will lead to different convexity. Thus, we discuss two cases, i.e., case $C_{2,k,n}^{(r)} \geq 0$ and case $C_{2,k,n}^{(r)} < 0$, respectively.

- When $C_{2,k,n}^{(r)} \geq 0$, the function $h_{3,k,n}^{(r)}(x[n],y[n])$ will be convex with respect to $x[n]$ and $y[n]$. In this case, we define the approximation for $h_{1,k,n}^{(r)}(d_k[n])$ as $h_{4,k,n}^{(r)}(x[n],y[n]) = h_{3,k,n}^{(r)}(x[n],y[n])$.
- When $C_{2,k,n}^{(r)} < 0$, the term $C_{2,k,n}^{(r)}((x[n]-w_{x,k})^2+(y[n]-w_{y,k})^2)$ will be concave in $x[n]$ and $y[n]$. According to the property of concave functions, we have

$$\begin{aligned} & h_{1,k,n}^{(r)}(d_k[n]) \leq h_{3,k,n}^{(r)}(x[n],y[n]) \\ \leq & \frac{C_{1,k,n}^{(r)}}{2}((x[n]-w_{x,k})^2+(y[n]-w_{y,k})^2)^2 + C_{2,k,n}^{(r)}(x^{(r)}[n]-w_{x,k})(2x[n]-x^{(r)}[n]-w_{x,k}) \\ & +C_{2,k,n}^{(r)}(y^{(r)}[n]-w_{y,k})(2y[n]-y^{(r)}[n]-w_{y,k}) + C_{3,k,n}^{(r)} \\ \triangleq & h_{4,k,n}^{(r)}(x[n],y[n]), \end{aligned} \tag{43}$$

  where $h_{4,k,n}^{(r)}(x[n],y[n])$ is clearly a convex function in $x[n]$ and $y[n]$.

With the defined $h_{4,k,n}^{(r)}(x[n],y[n])$ from the above discussions and recalling the inequality in (36c), we can obtain a convex approximation for function $\frac{1}{(\mathcal{F}_{\mathrm{A}}(\varphi_k[n]))^2}$

$$\frac{1}{(\mathcal{F}_{\mathrm{A}}(\varphi_k[n]))^2} \leq h_{1,k,n}^{(r)}(d_k[n]) + h_{2,k,n}^{(r)}(\mu[n]) \leq h_{4,k,n}^{(r)}(x[n],y[n]) + h_{2,k,n}^{(r)}(\mu[n]). \tag{44}$$

By combining the approximation (44) with the inequality in (25), we have the final concave approximation for harvested power as

$$\begin{aligned} \mathcal{F}_{\mathrm{nl}}\left(\frac{\beta_0 P N_t \mathcal{F}_{\mathrm{A}}(\varphi_k[n])}{d_k[n]^2}\right) & \geq -A_{1,k,n}^{(r)}\frac{F_{1,k,n}^{(r)}d_k[n]^4}{2} - A_{1,k,n}^{(r)}\frac{1}{2F_{1,k,n}^{(r)}\left(\mathcal{F}_{\mathrm{A}}(\varphi_k[n])\right)^2} + A_{2,k,n}^{(r)} \\ & \geq -A_{1,k,n}^{(r)}\frac{F_{1,k,n}^{(r)}d_k[n]^4}{2} - A_{1,k,n}^{(r)}\frac{h_{4,k,n}^{(r)}(x[n],y[n])+h_{2,k,n}^{(r)}(\mu[n])}{2F_{1,k,n}^{(r)}} + A_{2,k,n}^{(r)} \\ & \triangleq P_{k,n}^{(r)}(x[n],y[n],\mu[n]). \end{aligned} \tag{45}$$

where function $P_{k,n}^{(r)}(x[n],y[n],\mu[n])$ is concave and the inequality holds for any feasible point

$(x[n], y[n], \mu[n])$. Note that in each step of approximations, we have confirmed that the equality always hold at the local point $(x^{(r)}[n], y^{(r)}[n], \mu^{(r)}[n])$. Therefore, the equality in (45) must hold at the local point $(x^{(r)}[n], y^{(r)}[n], \mu^{(r)}[n])$.

So far, the tight concave approximation for harvested power has been constructed. By replacing the harvested power with its concave approximation, we can obtain a convex approximation (P3) for the problem (P2)

$$(\mathrm{P3}): \max_{\{x[n],y[n],\mu[n]\},E} \quad E \tag{46a}$$

$$\text{s.t.} \quad \sum_{n=1}^{N} P_{k,n}^{(r)}(x[n], y[n], \mu[n])dT \geq E, \ \forall k \in \mathcal{K}, \tag{46b}$$

$$(x[n+1]-x[n])^2+(y[n+1]-y[n])^2 \leq V^2 dT^2, \ \forall n \in \mathcal{N}, n \neq N, \tag{46c}$$

$$0 < \mu[n] \leq 1, \ \forall n \in \mathcal{N}. \tag{46d}$$

Since the problem (P3) is convex, an optimal solution for (P3) can be efficiently found via convex optimization tools, such as CVX and ellipsoid method [40].

With the convex approximation (P3), the problem (P2) is then enabled to be solved in an iterative manner. Next, we will clarify our proposed iterative algorithm for problem (P2).

C. Proposed Iterative Solution

In the initialization step, i.e., iteration index $r = 0$, we construct a feasible local point $(x^{(0)}[n], y^{(0)}[n], \mu^{(0)}[n])$. Then, in each iteration r, based on the local point $(x^{(r)}[n], y^{(r)}[n], \mu^{(r)}[n])$, we build the concave approximation $P_{k,n}^{(r)}(x[n], y[n], \mu[n])$ for the harvested power according to (45) and solve the convex problem (P3). After the the problem (P3) is optimally solved, the solution will be applied as the local point in the next (i.e., $r+1$-th) iteration. By repeating the iterations, the objective for problem (P2) will be constantly improved.

Note that the tight approximation in (45), which assures zero approximation error at local point $(x^{(r)}[n], y^{(r)}[n], \mu^{(r)}[n])$, guarantees an improvement of the objective value for problem (P2) in each iteration. In particular, in iteration r, the following relation holds at the local point

$$\begin{aligned}
&\min_k \left\{ \sum_{n=1}^{N} \mathcal{F}_{\text{nl}} \left(\frac{\beta_0 P N_t \mathcal{F}_{\text{A}}(\varphi_k^{(r)}[n])}{d_k^{(r)}[n]^2} \right) dT \right\} = \min_k \left\{ \sum_{n=1}^{N} P_{k,n}^{(r)}(x^{(r)}[n], y^{(r)}[n], \mu^{(r)}[n])dT \right\} \\
\leq \ &\min_k \left\{ \sum_{n=1}^{N} P_{k,n}^{(r)}(x^{(r+1)}[n], y^{(r+1)}[n], \mu^{(r+1)}[n])dT \right\} \\
\leq \ &\min_k \left\{ \sum_{n=1}^{N} \mathcal{F}_{nl} \left(\frac{\beta_0 P N_t \mathcal{F}_{\text{A}}(\varphi_k^{(r+1)}[n])}{d_k^{(r+1)}[n]^2} \right) dT \right\}.
\end{aligned} \tag{47}$$

Therefore, by repeating the iterations, the minimum harvested energy among all SNs is steadily increasing. Since the minimum harvested energy among SNs is upper-bounded, the solution cannot unlimitedly be improved and will eventually converge to a suboptimal point. Finally, from the solution, we can extract out the jointly optimized UAV trajectory $\{x[n], y[n]\}$ and directional antenna orientation scheme $\{\theta_0[n]\}$ according to $\theta_0[n] = \arccos \mu[n]$, $\forall n \in \mathcal{N}$.

D. Feasible Point Initialization

For iterative algorithm, especially in UAV trajectory design problem, the initialized point has much effects on the convergence speed and converged suboptimal solution. In this work, we perform an efficient UAV trajectory initialization, as partly described in [20].

First, we initialize a path for UAV trajectory by finding the shortest path connecting all SNs, i.e., by solving a Travelling Salesman Problem (TSP) [41]. Note that a suboptimal result of the TSP will be sufficient for the initialization step. Then, we examine the total length of the path. If the path length is longer than VT (the maximum travelling distance of the UAV), we shrink the total path to the centre of all SNs, i.e., $(\frac{\sum_k w_{x,k}}{K}, \frac{\sum_k w_{y,k}}{K})$, until the path length equals to VT. In this case, UAV trajectory is established by assuming the UAV flying along the path with maximum speed V. When the length of the initialized path is smaller than VT, to form the trajectory, the UAV is assumed to fly with a constant speed to finish the path with time length T. Afterwards, the initialized time-slot divided trajectory $\{x^{(0)}[n], y^{(0)}[n]\}$ is directly obtained from the initial continuous UAV trajectory. Furthermore, the initial elevation angle of directional antenna is initialized as $\theta_0^{(0)}[n] = \frac{\pi}{4}$, $\forall n \in \mathcal{N}$. Accordingly, the initial value of auxiliary variable $\mu[n]$ to be optimized in problem (P2) is defined as $\mu^{(0)}[n] = \cos \theta_0^{(0)}[n] = \frac{\sqrt{2}}{2}$, $n \in \mathcal{N}$.

After all, the flow of our proposed iterative algorithm for joint UAV trajectory and directional antenna orientation design, is displayed in Algorithm 1.

E. Complexity Analysis

In our proposed iterative algorithm, the computational complexity mainly results from solving the convex approximation of the original problem in each iteration. According to [23], the complexity of solving a convex problem is largely affected by the number of variables to be optimized and can be analyzed based on ellipsoid method [40]. In each iteration, we have considered a convex problem with $3N = \frac{3T}{dT}$ variables, including N UAV positions and N orientation variables, which has resulted a complexity of $\mathcal{O}(\frac{81T^4}{dT^4})$. By taking the iteration numbers

Algorithm 1 for jointly designing UAV trajectory and directional antenna orientation

Initialization

Initialize $\{x^{(0)}[n], y^{(0)}[n], \mu^{(0)}[n]\}$ according to Section III-D and set $r = 0$.

Iteration

a) Construct concave function $P_{k,n}^{(r)}(x[n], y[n], \mu[n])$ on point $(x^{(r)}[n], y^{(r)}[n], \mu^{(r)}[n])$ for all pairs of k and n;

b) Solve the convex problem (P3), obtain the optimal point $\{x^{(r\star)}[n], y^{(r\star)}[n], \mu^{(r\star)}[n]\}$;

c) **If** the objective improvement is below a threshold ϵ_{th}

Define the final solution as $\{x^{\star}[n], y^{\star}[n], \mu^{\star}[n]\} = \{x^{(r\star)}[n], y^{(r\star)}[n], \mu^{(r\star)}[n]\}$;

Calculate the corresponding elevation angle $\theta_0^{\star}[n] = \cos \mu^{\star}[n]$;

Stop the algorithm.

Else

$\{x^{(r+1)}[n], y^{(r+1)}[n], \mu^{(r+1)}[n]\} = \{x^{(r\star)}[n], y^{(r\star)}[n], \mu^{(r\star)}[n]\}$;

$r = r + 1$;

Go back to **a).**

End

into account, the overall complexity of the proposed algorithm can be summarized as $\mathcal{O}(\varepsilon \frac{81T^4}{dT^4})$, where ε denotes the iteration numbers required by the algorithm. Clearly, we can observe that a smaller time resolution dT will result in a dramatically increase in complexity, which has reveal the tradeoff between quantization accuracy and the computational complexity.

IV. Simulation Results

In this section, via simulations we evaluate our proposed modified antenna pattern and iterative algorithm for the maximization of minimum harvested energy among SNs. The average minimum harvested power within the charging period is treated as the key system performance indicator in the evaluation. The default parameter setups of simulations are provided as follows: First, the SNs are randomly distributed in a square area with width of 30m. In addition, we set $K = 5$, $H = 10$m, $N_t = 5$, $\beta_0 = -30$dB, $P = 40$dBm, $T = 50$s and $V = 1$m/s. Furthermore, the time resolution dT is set to $dT = 1$s and the modification factor in antenna pattern model is chosen as $\delta = 0.9$. Regarding the non-linear EH model, a group of parameters are inherited from [23] and [24], which are given by $I_s = 5\mu A$, $n_0 = 4$, $R_{ant} = 200\Omega$ and $nv_t = 1.05 \times 25.86$mV.

Following the parameterization, we in the following evaluate our proposed algorithm by discussing the convergence behaviour, spotlighting the advantages of operating WPT with directional antenna and observing the obtained result with different setups.

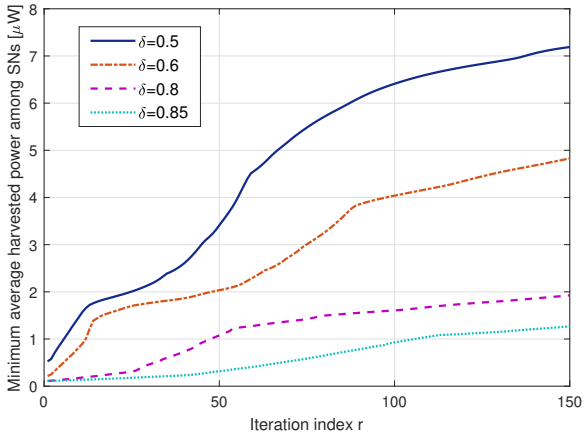

Fig. 4. Convergence behaviour with different modification factor δ.

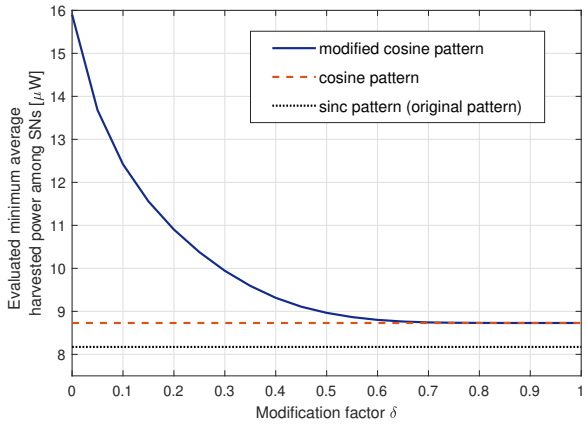

Fig. 5. WPT performance evaluation under different antenna pattern models.

A. Algorithm Convergence Validation

We first present the convergence speed with different modification factor δ, in Fig. 4. First, it can be observed that a smaller δ makes the algorithm converges faster. Recall that according to Fig. 3 and (16), a small δ indicates an inaccurate approximation of directional antenna pattern in comparison to the cosine antenna pattern. Combining this with the observation from Fig. 4, the factor δ actually introduces a tradeoff between the algorithm converge speed and the model accuracy, which needs to be carefully chosen.

To facilitate choosing the value of δ, we investigate the relationship between the estimated WPT performance (with the same solution from Fig. 4) and the choice of δ. The results are provided in Fig. 5. From the figure, we observe that in comparison to the accurate antenna pattern (i.e., the sinc pattern), both the cosine antenna pattern [32] and the proposed modified cosine pattern generally have small approximation errors, i.e., 1%. In particular, the approximation error of the cosine antenna pattern [32] is constant in δ, while the error of the proposed modified one decreases as δ increases and becomes considerable in the small value region of δ. From Fig. 5, we could conclude that the approximation error of the proposed modified cosine antenna pattern is as tiny as the original one [32] when we set $\delta \geq 0.8$.

It should be also pointed out that results in Fig. 4 and Fig. 5 do not indicate that a small value of δ is useless. Instead, they motivate us to effectively perform the iterative algorithm successively with different modification factors. More specifically, with a smaller δ, we can roughly iteratively optimize the problem efficiently, which can provide a high-quality initial point. Subsequently in the main iteration a larger δ is preferred to get an accurate result. In the

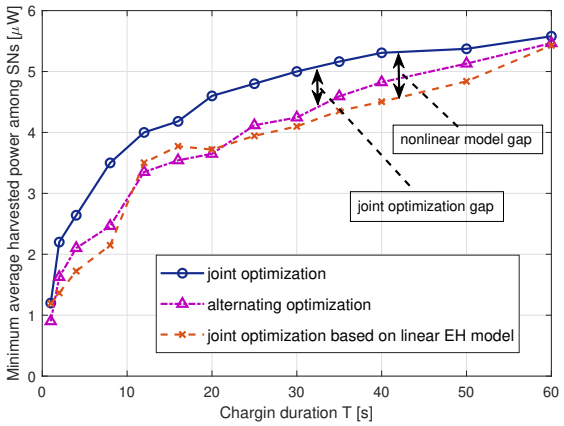

Fig. 6. WPT performance comparison under different optimization strategy.

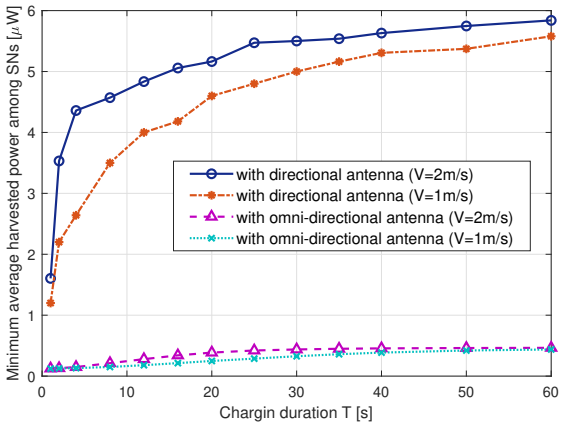

Fig. 7. WPT performance comparison with varying charging duration T.

following subsection evaluating the proposed joint design, we set $\delta = 0.5$ and $\delta = 0.9$ in the initialization and iterations, respectively.

B. Joint Design Evaluation

To evaluate the advantages of our proposed joint design, we consider the following three benchmarks:

- **Alternating optimization:** In alternating optimization, the UAV trajectory and the directional antenna are alternately optimized. Namely, the trajectory is optimized with fixed $\mu[n]$, while $\mu[n]$ is designed based on fixed UAV trajectory. Since the original problem is convex neither in trajectory nor in $\mu[n]$, we perform the alternating optimization on (P2) and iteratively update (P2) to obtain a converged suboptimal solution.
- **Joint optimization based on linear model:** While ignoring the nonlinear conversion in EH, which is assumed in most existing works, the joint design can be performed in the same way as our proposed design. Then, the WPT performance is evaluated based on the nonlinear model.
- **Design with omni-directional antenna:** With omni-directional antenna, only the UAV trajectory is required to be optimized, which can be done by modifying our proposed algorithm for the directional antenna case with $\mathcal{F}_{\mathrm{A}}(\varphi_k[n]) = 1$. An iterative algorithm can similarly constructed.

In addition, in all the following simulations in this subsection, the WPT performance, i.e., minimum average harvested power among SNs, is calculated via averaging over 10 random topologies (of SN distributions).

We start with Fig. 6 to compare the WPT performance from different algorithms, i.e., the proposed joint optimization, alternating optimization and the joint optimization based on linear model. With different charging duration T, our proposed joint designs always outperforms the other two benchmarks. Compares with alternating optimization, a joint optimization performance gap is marked in the figure and validates the advantages of our proposed joint design. Besides, in comparison with the result based on linear model, our design, which considers a nonlinear model, has shown clearly a much better average harvesting result, which illustrates the benefits for considering a nonlinear EH model for WPT network.

Then, we in Fig. 7 show the system WPT performance with different setups of charging duration T and UAV speed limit V and different antenna types. First, it can be found from the figure that for both cases with either a directional or an omni-directional antenna, a larger T and a larger V implies a better average WPT performance, i.e., minimum average harvested power among SNs. This is due to the fact that with a larger T, more time can be allocated for UAV staying at a position with a relatively higher WPT performance (possibly closer to the SNs). In addition, a larger V introduces a higher flexibility of UAV mobility, i.e., less time is spent for flying and more time can be used for hovering at a high performance position. Besides, we can also observe that the network with a directional antenna always outperforms that with an omni-directional antenna. As for reasons, the additional introduced antenna gain from the directional antenna has significantly compensated the pathloss in transmissions, so that more power can be wirelessly transferred with the optimized directional antenna orientation scheme. To sum up, increasing T or V are both able to improve the WPT performance. But the interesting part is that the performance improvement via increasing T or V is more significant in the directional antenna case in comparison to the omni-directional one. This observation suggests having relatively more fast UAV and more adequate charging duration for operating directional antenna UAV-enabled WPT network.

Corresponding to the Fig. 7, the trajectory difference between the directional antenna case and the omni-directional antenna case, and the directional antenna behaviour are provided in four subfigures of Fig. 8. First, from the trajectory comparison in Fig. 8(a) and Fig. 8(b), we find that the trajectory with a directional antenna tends to be closer to the SNs than that with an omni-directional antenna. This is due to the broadcasting channel property of the omni-directional antenna, under which the position closer to parts of the SNs does not necessarily result in a

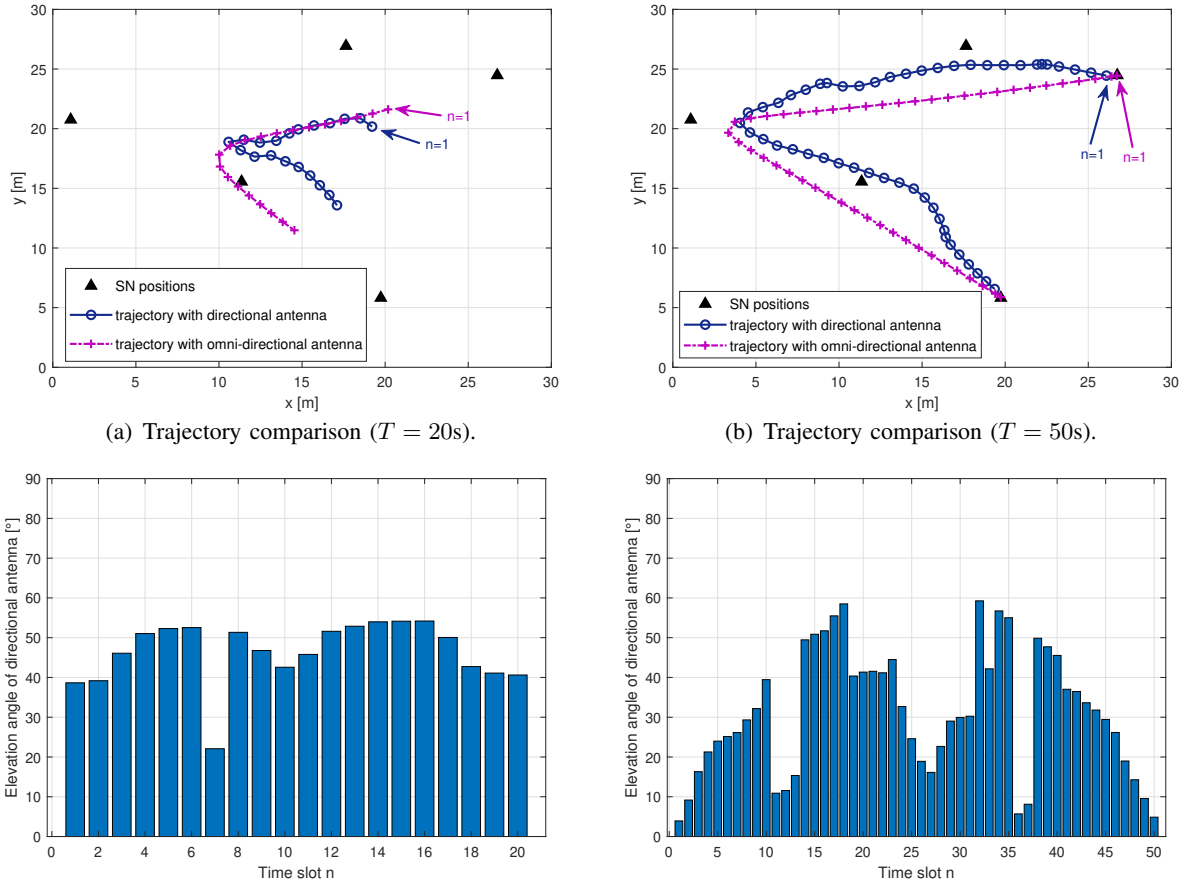

(a) Trajectory comparison ($T = 20$s).

(b) Trajectory comparison ($T = 50$s).

(c) Optimized elevation angle θ_0 ($T = 20$s).

(d) Optimized elevation angle θ_0 ($T = 50$s).

Fig. 8. Trajectory comparison and directional antenna orientation observation ($V = 1$m/s).

better (overall) performance, i.e., minimum average harvested power among SNs. By contrast, with a directional antenna, at each time instant the UAV is able to (and highly likely does) cover not all but parts of the SNs, which makes it fly closer to the covered SNs and orient the directional antenna towards these SNs to gain a higher performance. This is further confirmed in Fig. 8(c) and Fig. 8(d). When the horizontal distance between UAV and SNs are relatively larger, the optimized elevation angle for directional antenna turns to be larger to cover the SNs with main lobe. On the other hand, when the UAV is above a SN, the optimized elevation angle θ_0 approaches to zero to efficiently charge the targeted SN.

Next, we study the influence of UAV altitude H on the WPT performance in Fig. 9 and Fig. 10. We address relatively lower SN densities, i.e., $K = 5$ and $K = 10$ in a 30m$\times$30m square area, in Fig. 9, and relatively higher SN densities in Fig. 10 with $K = 20$ and $K = 40$. For both figures, we learn that a larger height H leads to a relatively lower average harvested power at SNs, since the pathloss will increase when UAV flies at a higher altitude. During the

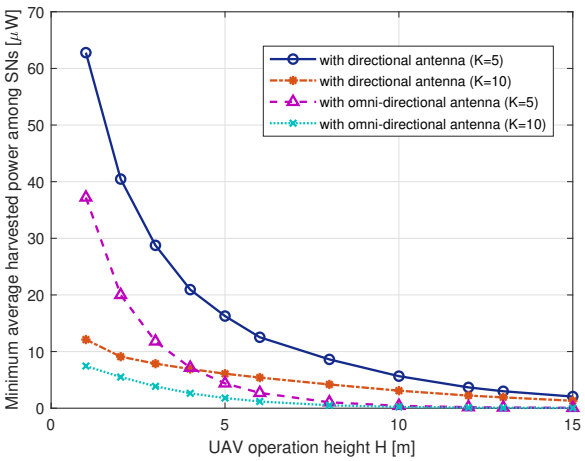

Fig. 9. WPT performance comparison with different height H and relatively lower SN density.

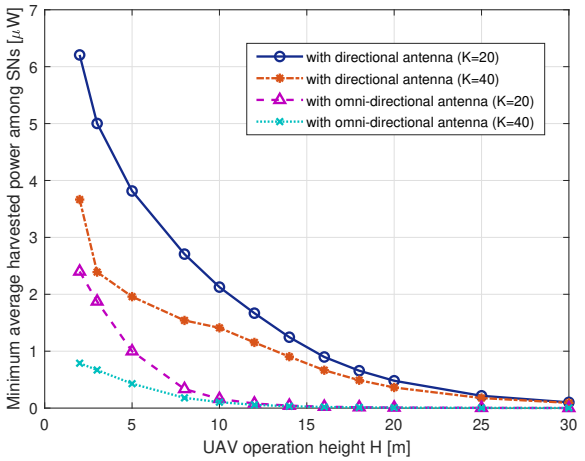

Fig. 10. WPT performance comparison with different height H and relatively higher SN density.

simulations, to get rid of the effect of randomness, when a larger K is deployed, we directly add new random SNs based on the scenario with a small K. Note that both the coverage (continuously providing the WPT service) and the signal strength directly and significantly influence the WPT performance. In addition, the directional antenna has shown a relatively narrow beamwidth when the number of antenna elements becomes larger, i.e., resulting in a narrow coverage in comparison to the omni-directional antenna. Hence, one would expect the dichotomy with respect to WPT performance between the omni-directional antenna case (with a better coverage performance) and the directional antenna case (providing a higher signal strength). However, we discover a very interesting result from Fig. 9 and Fig. 10 that for both the low-density and high-density SN scenarios, the system with a directional antenna always outperforms that with an omni-directional antenna. On the one hand, the reason is clear for the low SN density scenario: Based on the (trajectory and elevation angle) solutions provided in Fig. 8, with a relatively lower SN density the directional antenna is directly oriented to different SNs in each time slot, so that a much higher WPT performance is achieved in comparison to the omni-directional antenna case. On the other hand, for the high SN density scenario, where the coverage performance is more critical, it is essential to investigate why the directional antenna case always outperforms the omni-directional one, and how the coverage limitation of directional antenna is overcome.

The above observation motivates us to focus on the high density scenario and investigate the characteristics of the solutions (including the UAV trajectory, elevation angle and coverage of directional antenna) obtained via the proposed iterative algorithm. The results are provided in Fig. 11 and Fig. 12. In particular, we present in Fig. 11 the obtained UAV trajectory solution with

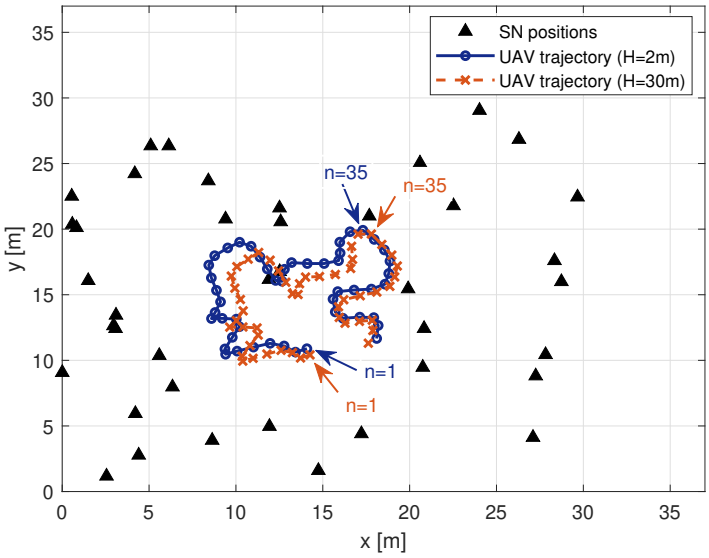

Fig. 11. Trajectory comparison at different height.

($K = 40$) and different UAV heights ($H = 2$m and $H = 30$m), and in Fig. 12 the corresponding solution of the directional antenna orientation. From the trajectory given in Fig. 11, we find that with different UAV heights, the UAV trajectory differs slightly. This is due to that to efficiently harvest the SNs, the optimized UAV trajectory largely relies on the distribution of SNs and the initial feasible point. In particular, when the UAV height is higher, the UAV positions along the trajectory are more concentrated. While operating at a larger height, the UAV will be capable of more easily providing a large coverage with directional antenna, so that slight position diversity is sufficient to make the UAV trajectory cover all SNs. Besides, by observing Fig. 12(a), we also find that with a UAV height of $H = 2m$, the optimized elevation angles for directional antenna orientation approach to 90 degrees, which implies the direction for main lobe in the directional antenna is close to the horizontal direction. Hence, the narrow main lobe is capable of covering a large area and serving more SNs. By contrast, in Fig. 12(b), due to the large vertical distance (i.e., larger H) from UAV to ground plane, a relatively smaller elevation angle is sufficient for gaining a large coverage. In particular, by taking the time slot $n = 35$ as an example, we display the corresponding distribution of harvested power with the optimized UAV position and directional antenna orientation at the heights of $H = 2$m and $H = 30$m, in Fig. 12(c) and Fig. 12(d), respectively. The harvested power distribution is clearly dominant by the antenna pattern and the distances from the UAV to the SNs. It should be mentioned that since a one-dimensional ULA can only perform a directional beamforming in the two-dimensional (2D) plane (implied in Fig. 2(b)), the projection of antenna pattern on the ground plane (i.e., coverage) has shown to

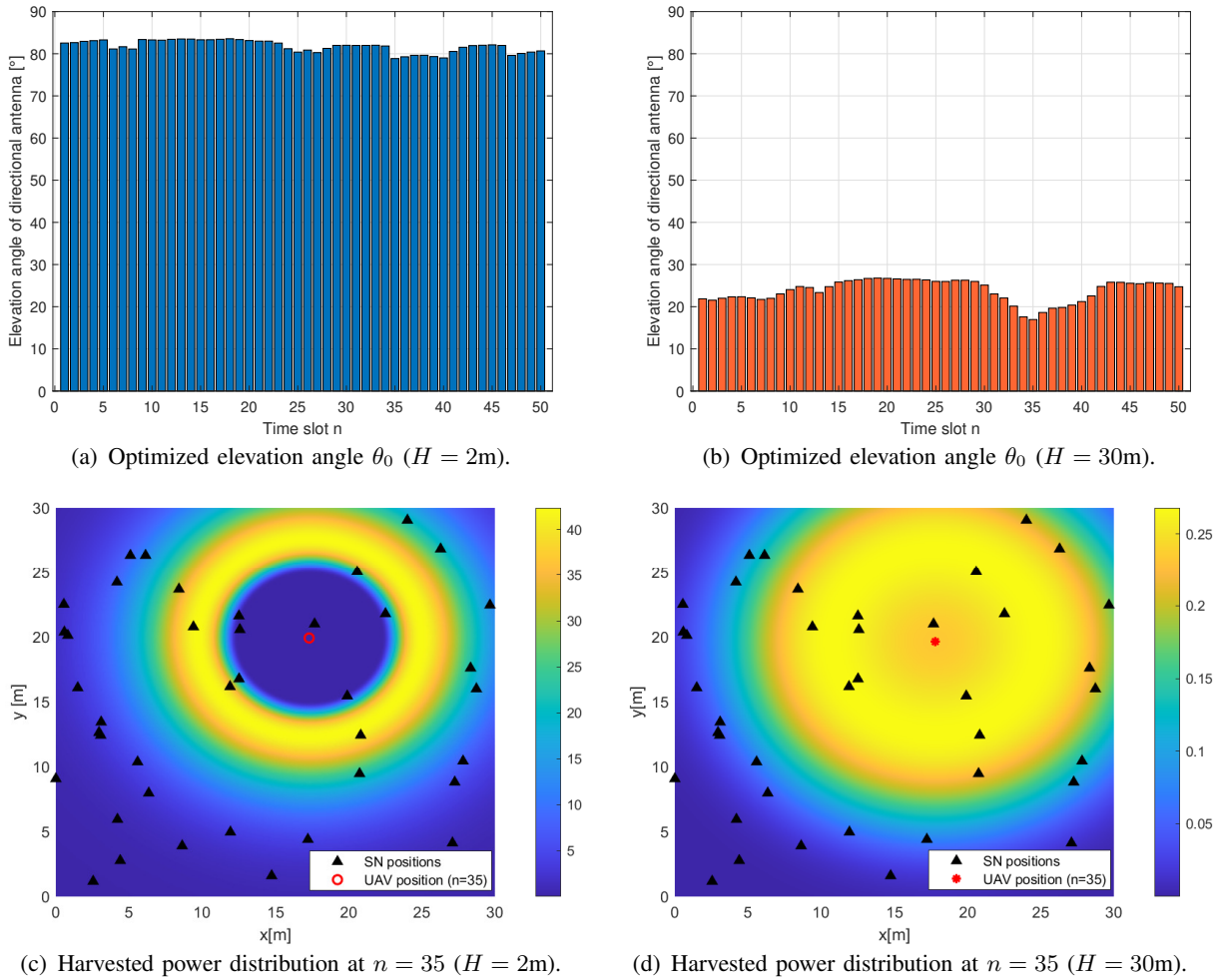

(a) Optimized elevation angle θ_0 ($H = 2$m).

(b) Optimized elevation angle θ_0 ($H = 30$m).

(c) Harvested power distribution at $n = 35$ ($H = 2$m).

(d) Harvested power distribution at $n = 35$ ($H = 30$m).

Fig. 12. Observation of optimized directional antenna orientation scheme ($K = 40$).

be a circular ring (as implied in Fig. 12(c) and Fig. 12(d)) instead of a circular area. According to Fig. 12(c), with a high SN density and a low UAV height, the SNs below and close to the UAV are not served in the such obtained solution of the directional antenna orientation. Instead, the solution turns to deploy the directional antenna by focusing on the corresponding coverage and the fairness among all SNs. By contrast, with a higher altitude ($H = 30$m) in Fig. 12(d), the directional antenna is oriented closer to the downward direction. With such characteristic, a sufficient coverage is guaranteed due to the larger operation height H of UAV. As a result, the directional antenna case achieves a higher WPT performance than omni-directional one.

Finally, we investigate the impact of antenna element number on the WPT performance, where we vary the UAV height H and SN numbers K in Fig. 13 and Fig. 14, respectively. As illustrated in the two figures, when the number of antenna elements increases, a higher WPT performance is generally achieved. This is due to the fact that a larger number of antenna elements directly

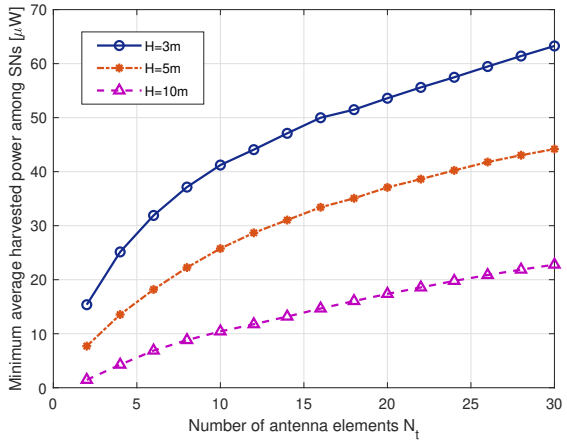

Fig. 13. Average performance with varying number of antenna elements and different height H.

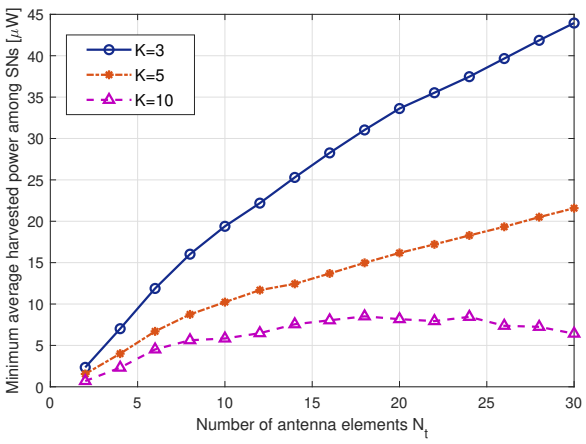

Fig. 14. Average performance with varying number of antenna elements and different SN number K

enlarges the maximum antenna gain and improves the received power at SNs. In addition, it is further confirmed with the observations in Fig. 7, Fig. 9 and Fig. 10 that a higher UAV height and a larger number of SNs result in a lower minimum harvested power among all SNs. Furthermore, we also notice that with relatively more SNs, e.g., $K = 10$, the performance improvement by increasing the number of antenna elements is significantly attenuated in comparison to the case with fewer SNs, i.e., the curve of $K = 10$ in Fig. 14 is more flat than the others. And when N_t is larger than 25, the corresponding WPT performance is even slightly decreased. The explanation is that increasing N_t does enhance the antenna gain but at the same time also makes the beam of the directional antenna narrower. As a result, when the number of antenna elements is already relatively large, i.e., the beam is already small, the bottleneck SNs likely benefit less from adding more antenna elements and even get harmed by the resulted narrow beam.

V. Conclusion

In this paper, we considered a UAV-enabled WPT network where a directional-antenna (array) is deployed on the UAV. We studied the WPT performance of the network, i.e., the minimum harvested energy among all ground SNs, under an analog beamforming model of a ULA on the directional antenna and a non-linear EH model. With a maximum speed limit and a given charging period, we considered a joint design aiming at maximizing the WPT performance via jointly optimizing the UAV trajectory and the elevation angle of the directional beamforming. To address the problem which contains an infinite number of variables, we reformulated it via quantizing the UAV trajectory in the time domain and tightly approximating the antenna pattern model for the antenna gain, thus having a reformulated non-convex problem. Afterwards, we

made efforts to approximate the harvested power to a concave lower-bound function, with which a tight convex approximation for the reformulated problem has been constructed, i.e., the problem can be solved iteratively via efficiently handling a convex optimization problem in each iteration. Finally, an algorithm has been provided presenting the whole initialization and iteration process effectively and efficiently solving the joint design problem.

Via simulations, we confirmed the convergence of the proposed algorithm and the adaptability of the introduced modified antenna pattern. By comparing to the case with omni-directional antenna, we have shown significant advantages of deploying a directional antenna in UAV-enabled WPT networks. Moreover, we investigated the behaviours of the proposed design under different setups of SN density and UAV height, and observe a very interesting result that the directional antenna is capable of overcoming the drawback of limited coverage when the UAV is operating at a low height. In particular, with a high SN density, the directional antenna at a low UAV operation height is optimized to orient at far points and to gain a large SN coverage.

We finalize the whole paper by underlining the extensionality of the methodologies and tools proposed in this work. This work for the first time proposed a joint optimization of directional antenna (directional beamforming) and UAV trajectory. The methodology of this combination highly likely assists also related joint designs and can be extended to varied scenarios with different system assumptions, like the scenarios with joint resource allocation including transmit power and the scenarios with SN position unknown and more practical channel model. In addition, to facilitate solving the joint optimization problem, we proposed a modified cosine antenna pattern which sufficiently approaches to the cosine antenna pattern and at the same time is simultaneously more analysable. Since we have adopted a one-dimensional ULA as the structure of directional antenna in this work, a further improvement by implementing a planar (2D) antenna array and three-dimensional (3D) antenna array can also be expected, where the modified cosine antenna pattern can also be applicable in these extensions. Third, during constructing the convex approximation of the considered problem, we proved and adopted a mathematical lemma for approximating a class of univariate functions to convex ones. This lemma can be applied also in other complex models and help in analysing the corresponding optimization problems, i.e., the problems can be tightly approximated and efficiently solved via similar iterative algorithms as this work.

APPENDIX A
PROOF OF LEMMA 1

Recall the inequality (27) to be proved:

$$h(\gamma) \leq \frac{c}{2}\gamma^2 + (h'(\gamma_0) - c\gamma_0)\gamma + h(\gamma_0) - \gamma_0 h'(\gamma_0) + \frac{c}{2}\gamma_0^2, \ \forall \gamma \in \mathcal{D}. \tag{48}$$

Clearly, the equality holds when $\gamma = \gamma_0$. In particular, when $\gamma = \gamma_0$, both sides of the (48) are equal to $h(\gamma_0)$. Then, to prove the inequality (48), we equivalently prove that under the assumptions in Lemma 1, the following function

$$\mathcal{H}(\gamma) = h(\gamma) - \left(\frac{c}{2}\gamma^2 + (h'(\gamma_0) - c\gamma_0)\gamma + h(\gamma_0) - \gamma_0 h'(\gamma_0) + \frac{c}{2}\gamma_0^2\right), \ \gamma \in \mathcal{D}, \tag{49}$$

satisfies $\mathcal{H}(\gamma) \leq 0$, $\forall \gamma \in \mathcal{D}$. The first-order and second-order derivatives of function $\mathcal{H}(\gamma)$ are respectively given by

$$\mathcal{H}'(\gamma) = h'(\gamma) - (c\gamma + h'(\gamma_0) - c\gamma_0), \tag{50}$$

$$\mathcal{H}''(\gamma) = h''(\gamma) - c. \tag{51}$$

By substituting γ with γ_0, we can easily obtain that $\mathcal{H}(\gamma_0) = 0$ and $\mathcal{H}'(\gamma_0) = 0$. According to the assumptions in Lemma 1, we have $\mathcal{H}''(\gamma) \leq 0$ holds and $\mathcal{H}'(\gamma)$ is continuous in $\mathcal{D}$, so that $\mathcal{H}'(\gamma)$ is a monotonically increasing function in $\mathcal{D}$. Taking the assumption of a continuous domain $\mathcal{D}$ into account, we have that

- when $\gamma < \gamma_0$, $\mathcal{H}'(\gamma) \leq \mathcal{H}'(\gamma_0) = 0$;
- when $\gamma \geq \gamma_0$, $\mathcal{H}'(\gamma) \geq \mathcal{H}'(\gamma_0) = 0$.

Therefore, the function $\mathcal{H}(\gamma)$ meets its maximum when $\gamma = \gamma_0$, i.e., $\mathcal{H}(\gamma) \leq \mathcal{H}(\gamma_0) = 0$, $\forall \gamma \in \mathcal{D}$.

REFERENCES

[1] Y. Zeng, R. Zhang, and T.J. Lim, "Wireless communications with unmanned aerial vehicles: Opportunities and challenges," *IEEE Commun. Mag.*, vol. 54, no. 5, pp. 36-42, May 2016.

[2] Q. Wu, Y. Zeng and R. Zhang, "Joint Trajectory and Communication Design for Multi-UAV Enabled Wireless Networks," *IEEE Trans. Wireless Commun.*, vol. 17, no. 3, pp. 2109-2121, March 2018.

[3] Y. Zeng, Q. Wu and R. Zhang, "Accessing From the Sky: A Tutorial on UAV Communications for 5G and Beyond," *Proceedings of the IEEE*, vol. 107, no. 12, pp. 2327-2375, Dec. 2019.

[4] L. Gupta, R. Jain and G. Vaszkun, "Survey of important issues in UAV communication networks," *IEEE Commun. Surveys Tuts.*, vol. 18, no. 2, pp. 1123-1152, SecondQuarter 2016.

[5] A. Al-Hourani, S. Kandeepan, and S. Lardner, "Optimal LAP altitude for maximum coverage," *IEEE Wireless Commun. Lett.*, vol. 3, no. 6, pp. 569–572, Dec. 2014.

[6] J. Lyu, Y. Zeng, R. Zhang, and T.J. Lim, "Placement optimization of UAV-mounted mobile base stations," *IEEE Commun. Lett.*, vol. 21, no. 3, pp. 604–607, Mar. 2017.

[7] R. Fan, J. Cui, S. Jin, K. Yang, and J. An, "Optimal node placement and resource allocation for UAV relaying network," *IEEE Wireless Commun. Lett.* , vol. 22, no. 4, pp. 808-811, Apr. 2018.

[8] P. Li and J. Xu, "Fundamental rate limits of UAV-enabled multiple access channel with trajectory optimization," *IEEE Trans. Wireless Commun.*, vol. 19, no. 1, pp. 458-474, Jan. 2020.

[9] Q. Wu and R. Zhang, "Common Throughput Maximization in UAV-Enabled OFDMA Systems With Delay Consideration," *IEEE Trans. Commun.*, vol. 66, no. 12, pp. 6614-6627, Dec. 2018.

[10] Y. Zeng and R. Zhang, "Energy-Efficient UAV Communication With Trajectory Optimization," *IEEE Trans. Wireless Commun.*, vol. 16, no. 6, pp. 3747-3760, June 2017.

[11] Y. Zeng, J. Xu, and R. Zhang, "Energy minimization for wireless communication with rotary-wing UAV", *IEEE Trans. Wireless Commun.*, vol. 18, no. 4, pp. 2329-2345, Apr. 2019.

[12] Y. Zeng, R. Zhang and T. J. Lim, "Throughput maximization for UAV-enabled mobile relaying systems," *IEEE Trans. Commun.*, vol. 64, no. 12, pp. 4983-4996, Dec. 2016.

[13] X. Zhou, Q. Wu, S. Yan, F. Shu and J. Li, "UAV-Enabled Secure Communications: Joint Trajectory and Transmit Power Optimization," *IEEE Tran. Veh. Technol.*, vol. 68, no. 4, pp. 4069-4073, April 2019.

[14] G. Zhang, Q. Wu, M. Cui and R. Zhang, "Securing UAV Communications via Joint Trajectory and Power Control," *IEEE Trans. Wireless Commun.*, vol. 18, no. 2, pp. 1376-1389, Feb. 2019.

[15] S. Zhang, H. Zhang, Q. He, K. Bian and L. Song, "Joint Trajectory and Power Optimization for UAV Relay Networks," *IEEE Commun. Lett.*, vol. 22, no. 1, pp. 161-164, Jan. 2018.

[16] N. Zhao, X. Pang, Z. Li, Y. Chen, F. Li, Z. Ding, and M.S. Alouini, "Joint Trajectory and Precoding Optimization for UAV-Assisted NOMA Networks," *IEEE Trans. Commun.*, vol. 67, no. 5, pp. 3723-3735, May 2019.

[17] Y. Hu, Y. Zhu, M. C. Gursoy, and A. Schmeink, "SWIPT-enabled relaying in IoT networks operating with finite blocklength codes." *IEEE J. Sel. Areas Commun.*, vol. 37, no. 2, pp. 1-16, Feb. 2019.

[18] S. Bi, C.K. Ho, and R. Zhang, "Wireless powered communication: Opportunities and challenges," *IEEE Commun. Mag.*, vol. 53, no. 4, pp. 117–125, Apr. 2015.

[19] X. Lu, P. Wang, D. Niyato, and D.I. Kim, "Wireless networks with RF energy harvesting: A contemporary survey," *IEEE Commun. Surv. Tut.*, vol. 17, no. 2, pp. 757-789, Secondquarter 2015.

[20] J. Xu, Y. Zeng, and R. Zhang, "UAV-enabled wireless power transfer: Trajectory design and energy optimization," *IEEE Trans. Wireless Commun.*, vol. 17, no. 8, pp. 5092–5106, Aug. 2018.

[21] Y. Hu, X. Yuan, J. Xu, and A. Schmeink, "Optimal 1D trajectory design for UAV-enabled multiuser wireless power transfer," *IEEE Trans. Commun.*, vol. 67, no. 8, pp. 5674-5688, Aug. 2019.

[22] X. Mo, Y. Huang, and J. Xu, "Radio-map-based robust positioning optimization for UAV-enabled wireless power transfer," *IEEE Wireless Commun. Lett.*, vol. 9, no. 2, pp. 179-183, Feb. 2020.

[23] X. Yuan, T. Yang, Y. Hu, J. Xu and A. Schemink, "UAV Trajectory Design for UAV-Enabled Multiuser Nonlinear Wireless Power Transfer," Early access, accepted by *IEEE Trans. Wireless Commun.*.

[24] B. Clerckx, R. Zhang, R. Schober, D. W. K. Ng, D. I. Kim, and H.V. Poor, "Fundamentals of wireless information and power transfer: From RF energy harvester models to signal and system designs," *IEEE J. Sel. Areas Commun.*, vol. 37, no. 1, pp. 4-33, Feb. 2019.

[25] E. Boshkovska, D.W.K. Ng, N. Zlatanov, and R. Schober, "Practical non-linear energy harvesting model and resource allocation for SWIPT systems," *IEEE Commun. Lett.*, vol. 19, no. 12, pp: 2082-2085, 2015.

[26] Y. Hu, X. Yuan, T. Yang, B. Clerckx, and A. Schmeink, "On the convex properties of wireless power transfer with nonlinear energy harvesting," *IEEE Trans. Veh. Technol.*, accepted. [Online]. Available: arXiv:1912.04785.

[27] H. Dai, K. Ng, R. C. Wong and M. Wu, "On the Capacity of Multi-Channel Wireless Networks Using Directional Antennas," *IEEE INFOCOM 2008 - The 27th Conference on Computer Communications*, Phoenix, AZ, 2008, pp. 628-636.

[28] I. Ahmed, H. Khammari, A. Shahid, A. Musa, K.S. Kim, E.D. Poorter, and I. Moerman, "A Survey on Hybrid Beamforming Techniques in 5G: Architecture and System Model Perspectives," *IEEE Commun. Surv. Tut.*, vol. 20, no. 4, pp. 3060-3097, Fourthquarter 2018.

[29] S. Kutty and D. Sen, "Beamforming for Millimeter Wave Communications: An Inclusive Survey," *IEEE Commun. Surv. Tut.*, vol. 18, no. 2, pp. 949-973, Secondquarter 2016

[30] Y. Wu, L. Qiu and J. Xu, "UAV-Enabled Wireless Power Transfer with Directional Antenna: A Two-User Case (Invited Paper)," *2018 15th International Symposium on Wireless Communication Systems (ISWCS)*, Lisbon, 2018, pp. 1-6.

[31] M. Mozaffari, W. Saad, M. Bennis and M. Debbah, "Efficient Deployment of Multiple Unmanned Aerial Vehicles for Optimal Wireless Coverage," *IEEE Commun. Lett.*, vol. 20, no. 8, pp. 1647-1650, Aug. 2016.

[32] X. Yu, J. Zhang, M. Haenggi and K. B. Letaief, "Coverage Analysis for Millimeter Wave Networks: The Impact of Directional Antenna Arrays," *IEEE J. Sel. Areas Commun.*, vol. 35, no. 7, pp. 1498-1512, July 2017.

[33] S. Li, B. Duo, X. Yuan, Y. Liang and M. Di Renzo, "Reconfigurable Intelligent Surface Assisted UAV Communication: Joint Trajectory Design and Passive Beamforming," *IEEE Wireless Commun. Lett.*, vol. 9, no. 5, pp. 716-720, May 2020.

[34] Q. Yuan, Y. Hu, C. Wang and Y. Li, "Joint 3D Beamforming and Trajectory Design for UAV-Enabled Mobile Relaying System," *IEEE Access*, vol. 7, pp. 26488-26496, 2019.

[35] C. Feng, C. Zhang and X. Luo, "Trajectory and Beamforming Vector Optimization for Multi-UAV Multicast Network," *2019 11th International Conference on WCSP*, Xi'an, China, 2019, pp. 1-6.

[36] L. Ge, P. Dong, H. Zhang, J. Wang and X. You, "Joint Beamforming and Trajectory Optimization for Intelligent Reflecting Surfaces-Assisted UAV Communications," *IEEE Access*, vol. 8, pp. 78702-78712, 2020.

[37] C. Bettstetter, C. Hartmann and C. Moser, "How does randomized beamforming improve the connectivity of ad hoc networks?," *IEEE International Conference on Communications*, Seoul, 2005, pp. 3380-3385 Vol. 5.

[38] Q. Wang, H.N. Dai, Z. Zheng, M. Imran, A.V. Vasilakos, "On Connectivity of Wireless Sensor Networks with Directional Antennas," *Sensors*, vol. 17, no.1, pp. 134, 2017.

[39] B. Clerckx and E. Bayguzina, "Waveform design for wireless power transfer," *IEEE Trans. Signal Proces.*, vol. 64, no. 23, Dec. 2016.

[40] S. Boyd. *EE364b Convex Optimization II, Course Notes*, accessed on Jun. 29, 2017. [Online]. Available: http://www.stanford.edu/class/ ee364b/

[41] H.A. Abdulkarim and I.F. Alshammari, "Comparison of algorithms for solving traveling salesman problem." *Int. J. Eng. Adv. Tech.*, vol.4, no.6, pp.76-79, Aug 2015.